

**DEUTSCHES ELEKTRONEN-SYNCHROTRON**

**Ein Forschungszentrum der Helmholtz-Gemeinschaft**

DESY 10-033

March 2010

**Scheme for generation of highly monochromatic  
X-rays from a baseline XFEL undulator**

Gianluca Geloni,

*European XFEL GmbH, Hamburg*

Vitali Kocharyan and Evgeni Saldin

*Deutsches Elektronen-Synchrotron DESY, Hamburg*

ISSN 0418-9833

**NOTKESTRASSE 85 - 22607 HAMBURG**

# Scheme for generation of highly monochromatic X-rays from a baseline XFEL undulator

Gianluca Geloni,<sup>a,1</sup> Vitali Kocharyan,<sup>b</sup> and Evgeni Saldin<sup>b</sup>

<sup>a</sup>*European XFEL GmbH, Hamburg, Germany*

<sup>b</sup>*Deutsches Elektronen-Synchrotron (DESY), Hamburg, Germany*

---

## Abstract

One goal of XFEL facilities is the production of narrow bandwidth X-ray radiation. The self-seeding scheme was proposed to obtain a bandwidth narrower than that achievable with conventional X-ray SASE FELs. A self-seeded FEL is composed of two undulators separated by a monochromator and an electron beam bypass that must compensate for the path delay of X-rays in the monochromator. This leads to a long bypass, with a length in the order of 40 – 60 m, which requires modifications of the baseline undulator configuration. As an attempt to get around this obstacle, together with a study of the self-seeding scheme for the European XFEL, here we propose a novel technique based on a pulse doubler concept. Using a crystal monochromator installed within a short magnetic chicane in the baseline undulator, it is possible to decrease the bandwidth of the radiation well beyond the XFEL design down to  $10^{-5}$ . The magnetic chicane can be installed without any perturbation of the XFEL focusing structure, and does not interfere with the baseline mode of operation. We present a feasibility study and we make exemplifications with the parameters of the SASE2 line of the European XFEL.

---

## 1 Introduction

The quality of the output radiation of X-ray SASE FELs is far from ideal because of the short longitudinal coherence length. This is a consequence of the fact that the process of amplification in a SASE FEL starts up from noise. The output radiation thus consists of a number of independent wavepackets (or spikes). As a rule, the length of each wavepacket is much shorter than

---

<sup>1</sup> Corresponding Author. Tel: ++49 40 8998 5450. Fax: ++49 40 8998 1905. E-mail address: gianluca.geloni@xfel.eu

the radiation pulse length and there is no phase correlation between the wavepackets. However, the improvement of the spectral brightness of an X-ray SASE FEL is of great practical importance, and has always been one of the goals of XFEL facilities. Due to the poor longitudinal coherence of the output radiation of conventional XFELs [1]-[5], an increase up to two order of magnitude (i.e. up to full longitudinal coherence) is, in principle, possible.

The self-seeding scheme [6], first proposed in the VUV and soft X-ray region makes use of a grating monochromator, and allows one to monochromatize radiation within an active frequency-filtering process, where the bandwidth is narrowed during, and not after the amplification process. The implementation of such scheme for the Angstrom wavelength range would take advantage of a crystal monochromator [7]. The presence of the monochromator introduces a path delay with respect to the straight path, which has to be compensated with the introduction of a long electron beam bypass in the order of 40 – 60 m for the case of an XFEL. As a result, this self-seeding scheme is not compatible with the baseline XFEL design presented in technical design reports [1, 2], and cannot be implemented in the very initial stage of operation.

In this paper we propose a way to obtain a similar result without interfering with the baseline mode of operation of the XFEL. We will show how, based on a pulse doubler concept, one can use a crystal monochromator installed within a short magnetic chicane in the baseline undulator to decrease the bandwidth of radiation well beyond the XFEL design, down to  $10^{-5}$ . The scheme can also work in combination with a fresh bunch technique, both for short (6 fs) and long (60 fs) pulse mode of operation. In the following section we will revisit the self-seeding scheme proposed in [7] (which will be named here "single bunch self-seeding scheme") for the case of beam parameters experimentally demonstrated [3, 4] at LCLS, and we will discuss our novel method (which will be named here "double bunch self-seeding scheme"). Further on, we will discuss a feasibility study for our new double bunch self-seeding technique, which may be used to enable the single bunch self-seeding technique as well. We present studies both for short and long pulse mode of operation.

## single bunch self seeded scheme

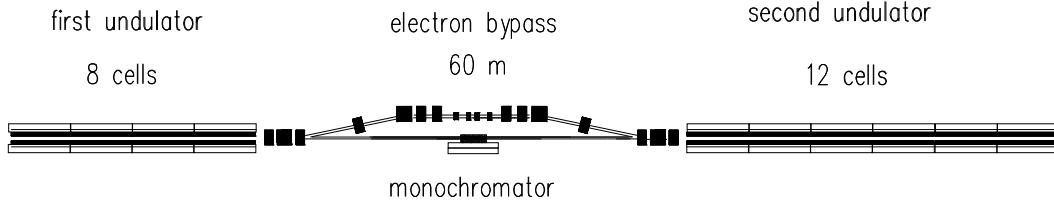


Fig. 1. Design of the undulator system for narrow bandwidth mode operation. The scheme is based on the use of single bunch self seeded technique

## 2 Methods for controlling the X-ray pulse linewidth

### 2.1 Single bunch self-seeding scheme

A self-seeded FEL [6]-[10] is composed of two undulators separated by a monochromator and an electron beam bypass, which washes out the microbunching and compensates for the path delay of X-rays in the monochromator, without significantly increasing the overall length of the bunch. Radiation in the linear regime is filtered through the monochromator, as the electron beam passes through the bypass. Further on, the monochromatized radiation seeds the washed out electron beam in the second undulator, and narrowband radiation, beyond the XFEL design, is produced. A schematic of the setup for the European XFEL is shown in Fig. 1. In the original VUV-soft X-ray case, a grating monochromator was proposed [6]. In the hard X-ray case a crystal monochromator should be used instead [7].

In the wavelength range around 0.1 nm, radiation undergoes an extra-path length in the order of at least a centimeter, due to the minimal transverse displacement between crystals in the monochromator. Such extra-path length is in the same order of that foreseen for the VUV self-seeding option at FLASH [9]. As mentioned above, the bypass both compensates for this path delay and washes out the electron beam microbunching.

For an energy spread of order  $\Delta\gamma/\gamma \sim 0.01\%$ , and wavelengths in the order

electron bypass for single bunch self seeded scheme

length 60 m

extra path length 1 cm

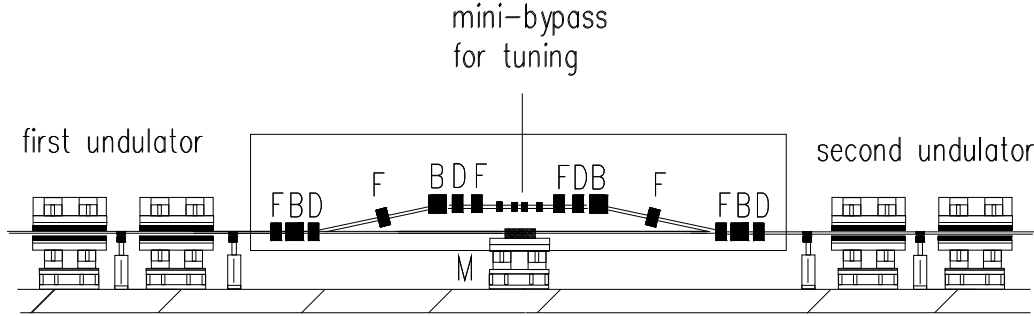


Fig. 2. Layout of the electron bypass. F - focusing quadrupole, D - defocusing quadrupole, B - bypass bending magnets, M - crystal monochromator.

of 0.1 nm, the electron beam microbunching is washed out already for an  $R_{56}$  in the order of a few microns. In the case of a four-magnet chicane with extra path length  $\delta L$  the dispersion is simply given by  $R_{56} = 2\delta L$ . This result does not depend on the distance between second and third magnet, which, due to technical reasons, can be comparable with the distance between first and second magnet. In our case, this distance is about 20 m. Without a special focusing system, the bypass should have a very large  $R_{56}$  in the order of a few centimeters. The bypass system should be nearly dispersion free, with matched beta functions at the entrance and at the exit, and should include the possibility of fine tuning the extra path length. Such setup, adapted from [9] for the XFEL case, is schematically presented in Fig. 2. Given the bending angle of the bypass magnets of about 2 degrees, the total length of the bypass is about 60 m.

An important point to be considered when studying the implementation of the self-seeding scheme is that heat-loading problems are not automatically avoided when a crystal monochromator is used at the European XFEL. In fact, while the power incident on the crystal is reduced of two orders of magnitude, the beam area inside the undulator is smaller of two orders of magnitude, as is illustrated in Fig. 3, leading to the same power density on the crystal. The situation changes when one considers e.g. the case of the LCLS near experimental hall, Fig. 4. First, in general, at LCLS one deals with a much lower repetition rate. Moreover, in the near hall the radiation spot size is still comparable with the spot size inside the undulator. Therefore, the power density on the crystal is reduced of two orders of magnitude if the monochromator is placed inside the undulator. Thus, heat-loading

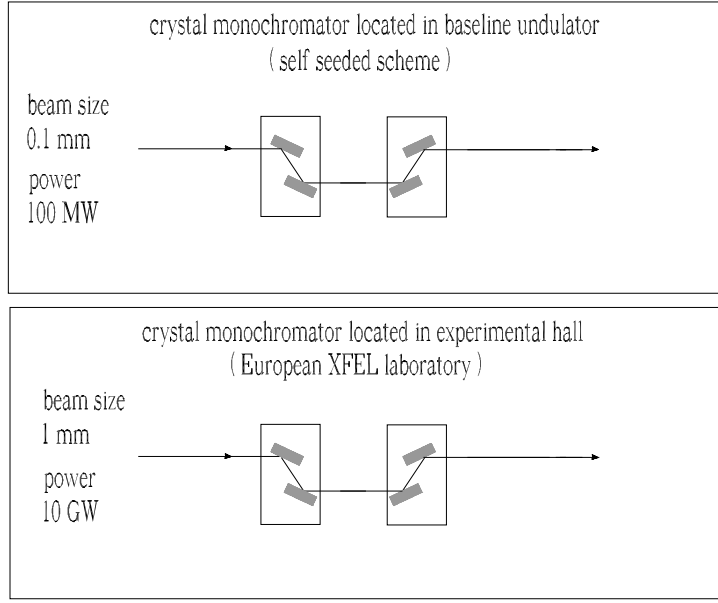


Fig. 3. An X-ray crystal monochromator will be required to reduce the bandwidth of the FEL for various applications, in particular for spectroscopy. A monochromator can be located in the baseline undulator (self-seeding scheme, upper picture) or in the experimental hall (bottom picture), with the self-seeding monochromatization improving the spectral brightness of two orders of magnitude. Comparing both geometries for the European XFEL case in relation with heat-loading problem, one finds that the power density in the experimental hall is practically the same as the power density in the self-seeding scheme.

problems are completely avoided using the self-seeding scheme. From this viewpoint, it should also be noted how the situation differs in the VUV case, where a grating monochromator is used as explained in [6]. In this case the resolution depends on the spot-size on the grating, Fig. 5. Once the resolution is fixed, the spot-size on the grating is fixed too, independently of the distance between undulator and experimental hall. As a result, in the self-seeding scheme for the VUV range, heat loading issues are relaxed of two or three orders of magnitude. Therefore, installing a crystal monochromator in the undulator always leads to an improvement in terms of spectral brightness, but advantages concerning heat loading problems depend on the situation. There are always advantages when considering the VUV case, but not always when dealing with XFELs.

## 2.2 Double bunch self-seeding scheme

As an alternative to the single-bunch self-seeding scheme we suggest a novel technique based on the creation of two identical electron bunches separated by the RF period  $T_0$  of the accelerating system used. The scheme

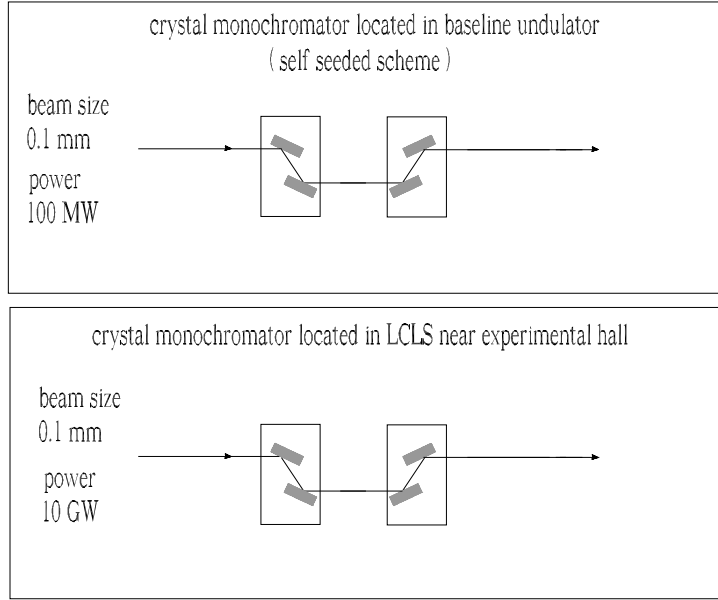


Fig. 4. Comparing the same geometries in Fig. 3 for the LCLS case in relation with heat-loading problems. The monochromatization in the self-seeding scheme (upper picture) is performed at much lower power density level with respect to monochromatization in the near experimental hall (lower picture).

grating monochromator

to obtain maximal resolution, we must have spot of radiation on the grating position of at least the size  $D \cos(\alpha)$

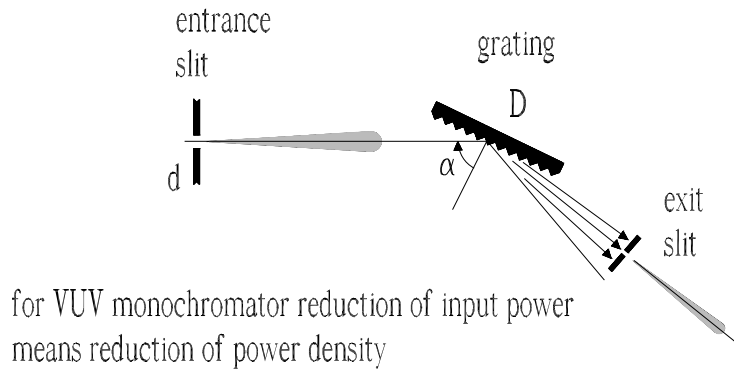


Fig. 5. Illustration of a grating monochromator principle. In the VUV range, the heat-load (both power and power density) on the grating monochromator is two or three orders of magnitude less than on a monochromator installed in the experimental hall, independently of the distance between undulator and experimental hall.

requires limited hardware, which can be installed in place of a single 5 m-long undulator module. Therefore, it does not perturb the baseline mode of

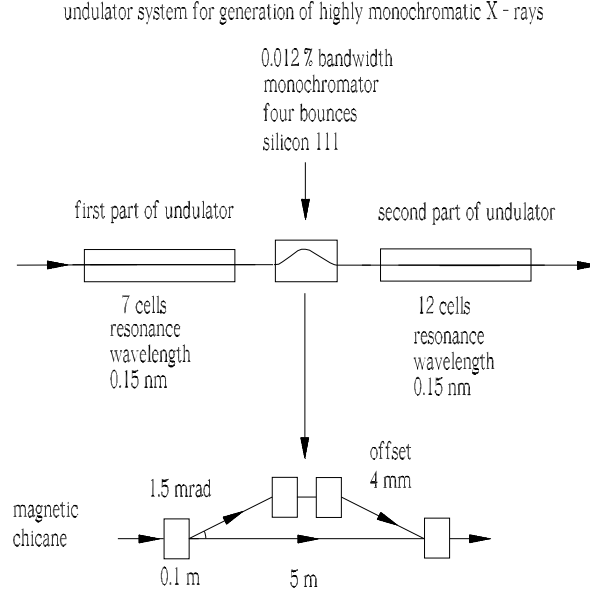


Fig. 6. Design of an undulator system for highly monochromatic X-ray source

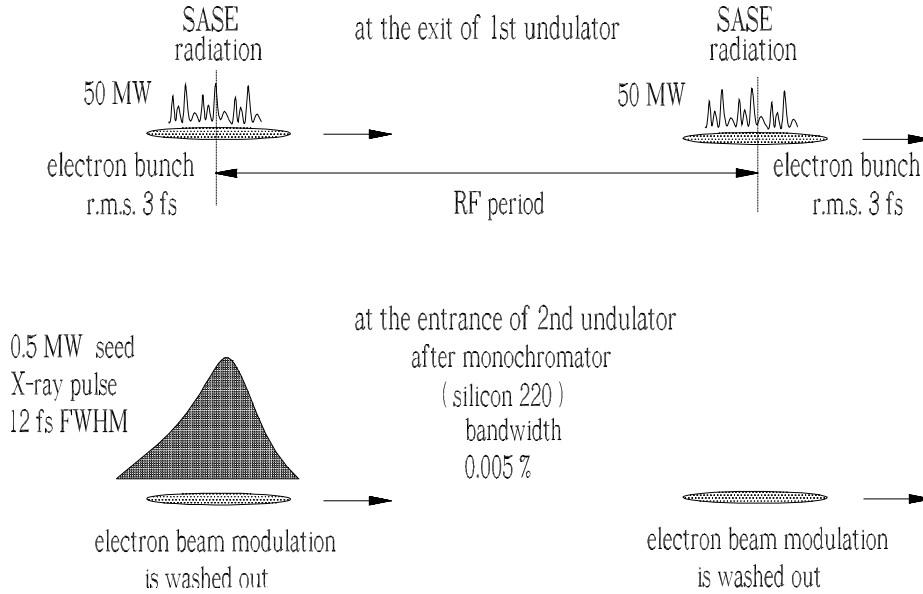


Fig. 7. Sketch of highly monochromatic X-ray pulse synthesis through double electron bunch generation and spectral filtering.

operation of the facility. In the case of short bunches<sup>2</sup>, the overall idea is sketched in Fig. 6 and Fig. 7, while the installation position of the magnetic chicane in the baseline undulator of an XFEL is shown in Fig. 8. Two short (3 fs rms) bunches, separated one from another of a temporal interval  $T_0$ , travel through the first part of the undulator (7-cells long at a resonance wavelength of 0.15 nm in the example in the figure), and start lasing from

<sup>2</sup> The method also works for long electron bunches as discussed later on.



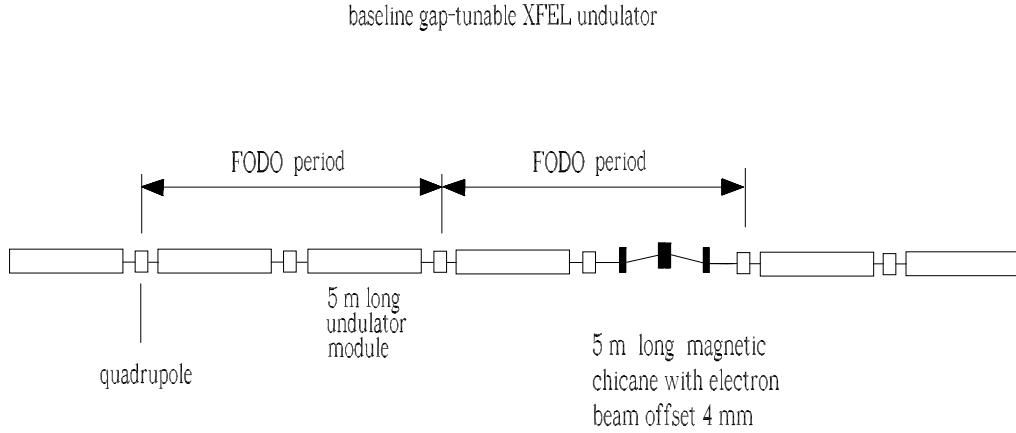


Fig. 8. Installation of the magnetic chicane in the baseline XFEL undulator. The magnetic chicane absolves two tasks. First, it allows for the installation of the monochromator. Second, the strength of the magnetic chicane as a dispersive section is sufficient for suppression of the beam modulation.

shot noise in the linear regime, producing pulses in the 50 MW level. Subsequently, they pass through a short magnetic chicane installed in place of a single module. The chicane has a deflection angle of 1.5 mrad and a length of 5m and has two purposes<sup>3</sup>. First, it washes out the beam microbunching ( $R_{56} \approx 11\mu\text{m}$  is more than enough to this purpose). Second it creates an offset of 4 mm, where we plan to install a four-bounce crystal monochromator. The monochromator filters the radiation from the first electron bunch, and it introduces a long path difference corresponding to the time  $T_0$ . Thus, at the entrance of the second undulator, the second electron bunch is seeded with an almost longitudinally-coherent seed.

The method requires the development of a photoinjector setup making use of a laser-pulse doubler concept like the one sketched in Fig. 9. The laser pulse to be used is split and delayed. A Michelson interferometer can be used to provide sub-micron accuracy control of the delay between the two split pulses, and enables a separation delay  $T_0$ . The two pulses are then sent to the photoinjector setup, as in Fig. 10, and two identical electron bunches, delayed of  $T_0$ , are created. A pioneering experiment for integrating the laser pulse doubler with an XFEL photoinjector was performed at FLASH. Results, which should be considered as first steps into a novel direction of

<sup>3</sup> A third effect is to delay the electron bunches relative to the radiation pulse of a short time (in the 10 fs range) which may be useful later on to finely tune the system by effect.

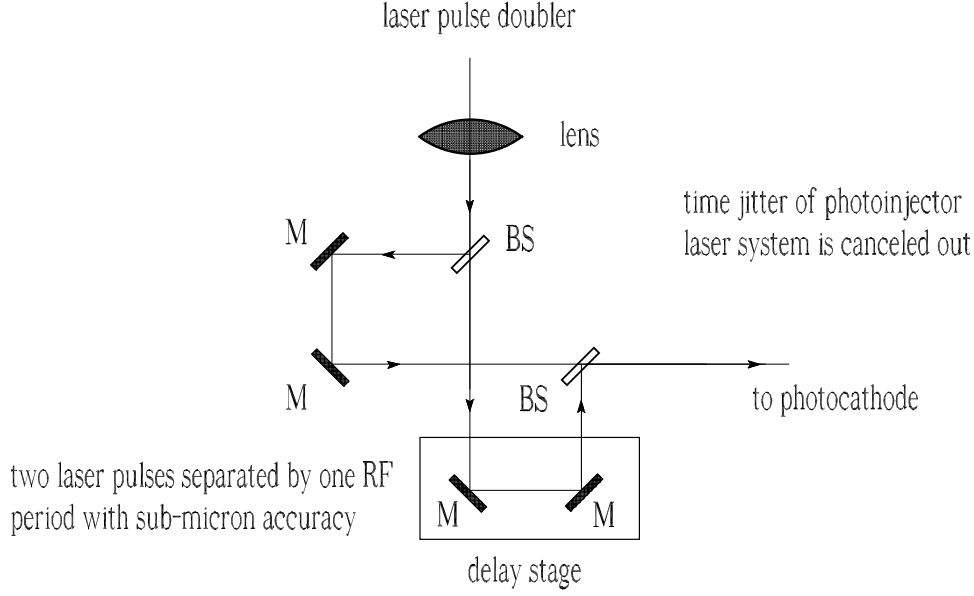


Fig. 9. Concept of laser pulse doubler. A Michelson interferometer provides control of the delay between two copies of the input laser pulse with sub-micron accuracy. Pulse separation is the RF period  $T_0$ .

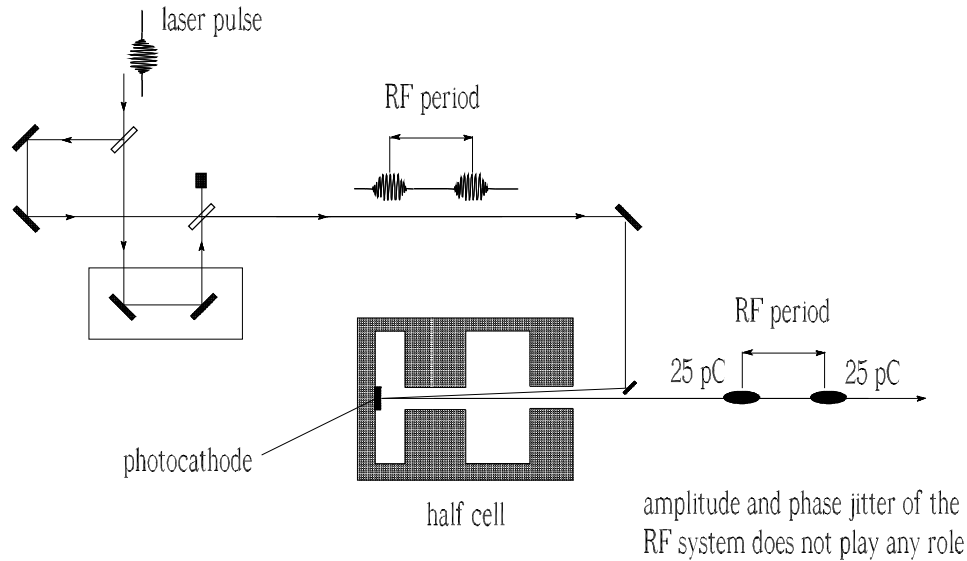


Fig. 10. Illustrative view of the proposed photoinjector setup using a laser pulse doubler.

XFEL technology, are reported in [11].

Usually, two main sources of time jitter between bunches are present: first, phase and amplitude jitter of the RF system. Second, time jitter of the photoinjector laser system. Since bunches are only one RF period apart, the jitter of the RF system does not play any role. Also, in our scheme the jitter

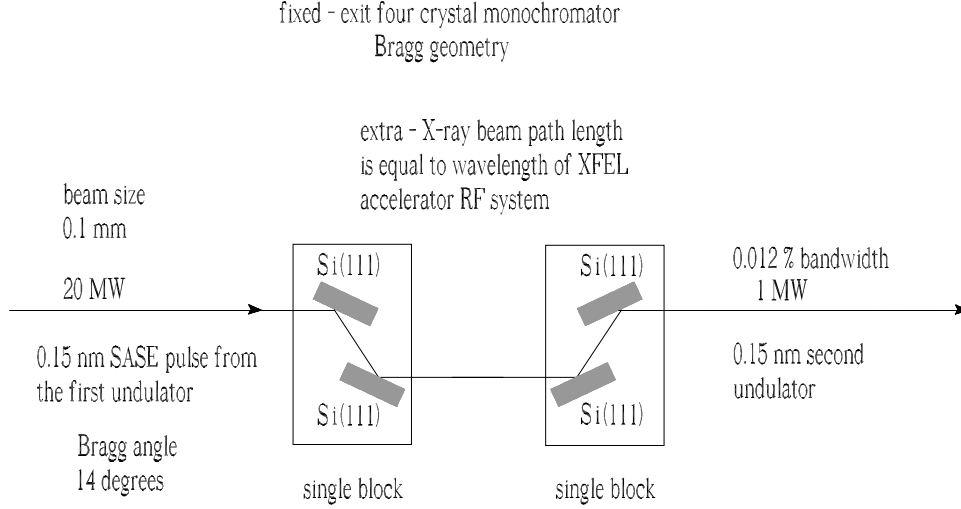


Fig. 11. Fixed-exit four-crystal monochromator: Silicon 111 reflection. The additional path length acquired by the X-rays in the monochromator is equal to wavelength of XFEL accelerator RF system.

of the photo injector laser system is cancelled out because we produce two laser pulses by splitting a single input laser pulse. As a result, the distance between the two laser pulses can be fixed with sub-micron optical accuracy. Moreover, due to the single-pulse splitting, we automatically have identical longitudinal pulse shapes, and the identity of the energy and of the transverse shape can be controlled with optical accuracy too, at least up to 0.1%. Finally, the low charge mode of operation works with charges (25 pC) which are 40 times smaller compared with the design value (1 nC). This allows one to neglect wakes of the first bunch on the second. However, we will demonstrate that our scheme enables a relatively large jitter acceptance up to tens rms of the electron bunch length.

The low charge mode of operation includes an additional technical advantage, because the photoinjector laser system can work, in this case, with laser pulses yielding an energy an order of magnitude smaller than those needed for the baseline mode of operation. therefore, no upgrade of the photoinjector laser system is needed, meaning that we propose a cost effective solution of the line-width control problem.

A key component of the proposed setup is the X-ray monochromator. We have chosen a four-bounce scheme as shown in Fig. 11. This solution is advantageous because it allows one to keep the exit direction and position of the X-ray beam equal to the entrance direction and position. In the monochromator, the X-ray pulse acquires a path delay given by  $\Delta L = 2H \tan(\theta_{nkl})$ , where  $H$  is the beam shift, and  $\theta_{nkl}$  is the Bragg angle of

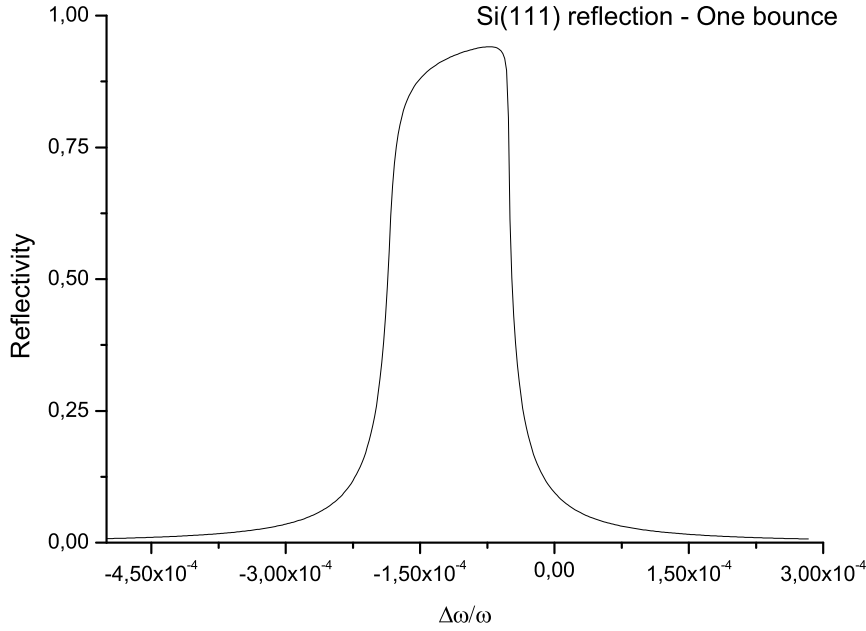


Fig. 12. Reflectivity curve for a thick absorbing crystal in Bragg geometry. Si(111) reflection of 0.15 nm X-rays. One bounce.

the reflections in the monochromator. Note that this relation is valid also in the case of back-reflections, i.e. for  $2\theta_{nkl} > \pi/2$ . By varying  $H$  one can keep the delay  $\Delta L$  constant in the whole tunability range of the monochromator.  $\Delta L$  should be chosen in such way that the total time delay of the radiation with respect to the electron beam, inclusive of corrections due to the presence of the magnetic chicane, equals  $T_0$ .

Multiple reflections result in a reduction of the tails of the reflectivity curve. Namely, if  $I(\omega)$  is the reflectivity curve for the single crystal, the reflectivity after  $N$  reflections is given by  $I^N(\omega)$ . Fig. 12 and Fig. 13 show the reflectivity curves for Silicon 111, respectively after one and four reflections, at  $\lambda = 0.15$  nm. The tails of the reflectivity curve decrease very rapidly with the number of reflections, due to the fact that the tails behave asymptotically as  $(\Delta\lambda/\lambda)^{-2}$ , after one reflection and as  $(\Delta\lambda/\lambda)^{-8}$  after four. However, the width of the curve remains constant. It should be noticed that here we discuss about silicon crystals only. There are two reasons for this. First, the main advantage of silicon is the availability of almost perfect synthetic monocrystals with high-reflectivity, thanks to semiconductor-industry demands. Second, silicon has the advantage of a high heat-conductivity and a high damage threshold, and can thus achieve good performance at high power load. As is well known, if the crystal plate is cooled, the thermal deformation results in a slope error composed of two components: a bending and a bump.

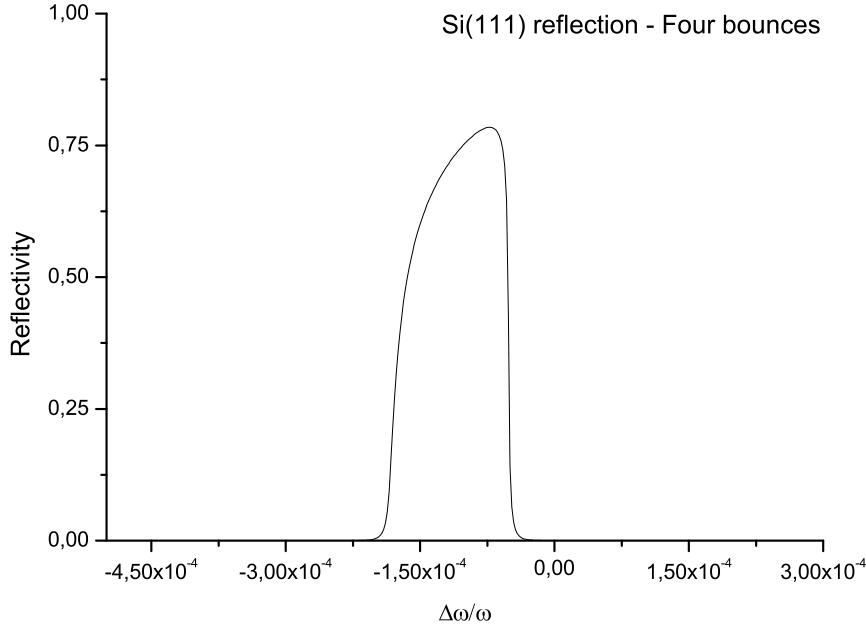


Fig. 13. Reflectivity curve for a thick absorbing crystal in Bragg geometry. Si(111) reflection of 0.15 nm X-rays. Four bounces.

The thermal deformation of the crystal induced by heat load depends on the ratio  $\alpha/k$ ,  $\alpha$  being the thermal expansion coefficient and  $k$  the thermal conductivity of the crystal, and for silicon it strongly depends on temperature, being zero at 125 K. This is the best high-power working point for the crystal. Lowering the temperature of silicon from room temperature to liquid-nitrogen temperatures improves the ratio  $k/\alpha$  by a factor 50.

The advantages of our scheme with respect to the single-bunch self-seeding method are obvious. The hardware needed here can be installed without perturbation of the baseline parameters, and switching to the normal SASE mode of operation is achieved by switching off the magnetic chicane and retracting the monochromator. Also, although it requires the development of a pulse doubler, it avoids complications and costs associated with the development of a dispersion-free 60-m long bypass. Wakefields problems, due to the influence of the passage of the first bunch on the second should be negligible for a low-charge mode of operation, while they deserve better attention in the long-pulse mode. Note that the time jitter acceptance for the double bunch scheme increases when the bandwidth of the monochromator decreases. Simultaneously, the seeding power decreases too, but it should be much larger than the shot noise power. Since the effective shot noise power is about 3 kW and the seeding power should be larger than 100 kW, for the short pulse mode of operation we are limited to Si(111) and Si(220)

combination of double bunch self-seeding technique and fresh bunch technique

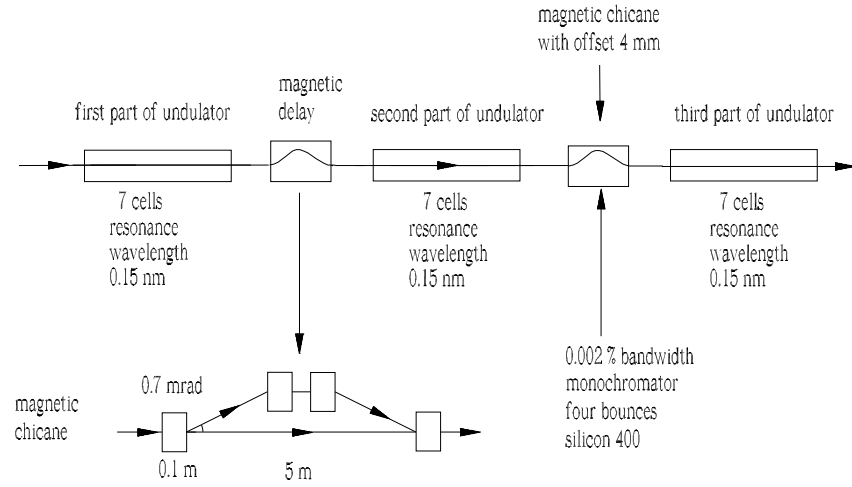


Fig. 14. Design of an undulator system for generation of highly monochromatic X-ray pulses. The method is based on a combination of the double-bunch self-seeding scheme and of the fresh-bunch technique.

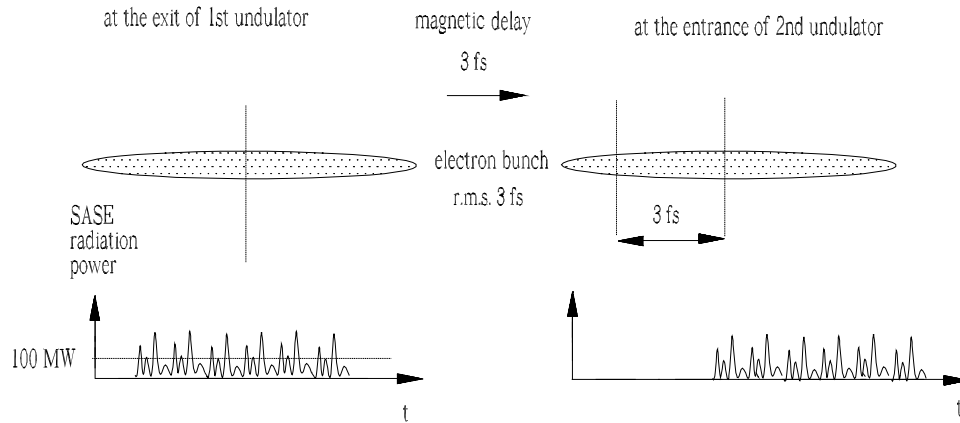


Fig. 15. Sketch of principle of fresh bunch technique for short (6 fs) pulse mode operation.

reflections. The situation changes combining the double bunch scheme with other recently introduced techniques, as discussed below.

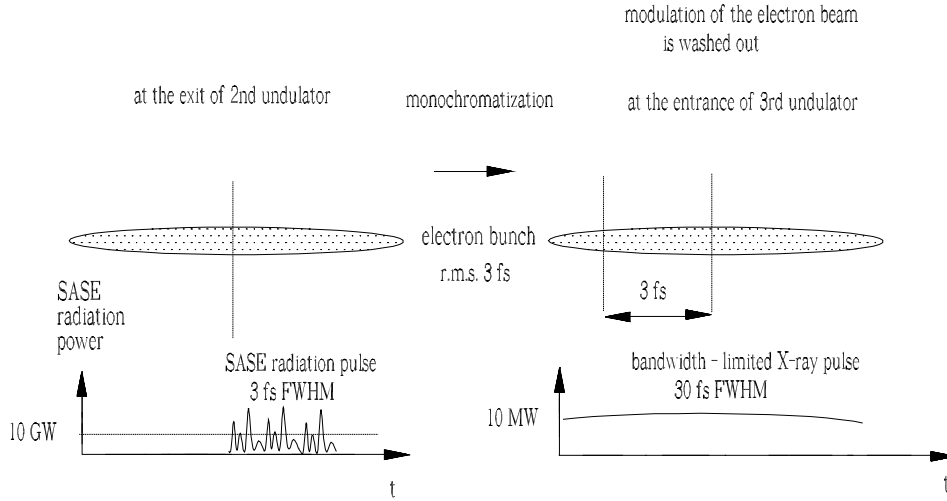


Fig. 16. Sketch of the X-ray monochromatization principle from second to third undulator. By using a combination of self-seeding and fresh bunch techniques, a 30 fs, monochromatic radiation can be produced behind the monochromator.

### 2.3 Combination of self-seeding scheme and fresh bunch technique

The method described above may be combined with a fresh bunch technique [12]-[19]. The idea is sketched in Fig. 14, Fig. 15 and Fig. 16. Compared to the previous scheme, this method makes use of the space occupied by two undulator segments, Fig. 14. After the first undulator part, where they undergo the SASE process in the linear regime, the two short (6 fs) electron bunches created with the pulse doubler described above are sent to a weak chicane, which washes out the microbunching and introduces a relative delay of the electron bunch compared to the radiation, Fig. 15. Then, half of the delayed electron bunches are seeded by their own radiation, and go up to saturation in the second undulator part. Finally, the strong radiation pulse at the end of the second undulator part is stretched by the crystal monochromator, see Fig. 16 and seeds the remaining, fresh part of the second electron bunch.

The combination of self-seeding and fresh-bunch technique brings mainly two advantages when dealing with the short pulse mode of operation. These are summarized in Fig. 17, which compares the two self-seeding schemes considered in this paper. The first advantage is constituted by the fact that the seeding power is increased due to the use of the fresh-bunch technique. Therefore, one can operate with monochromators with the smallest bandwidths (Silicon 400 and Silicon 440). This brings the advantage of increasing the jitter acceptance up to 20 rms lengths of the short bunch.

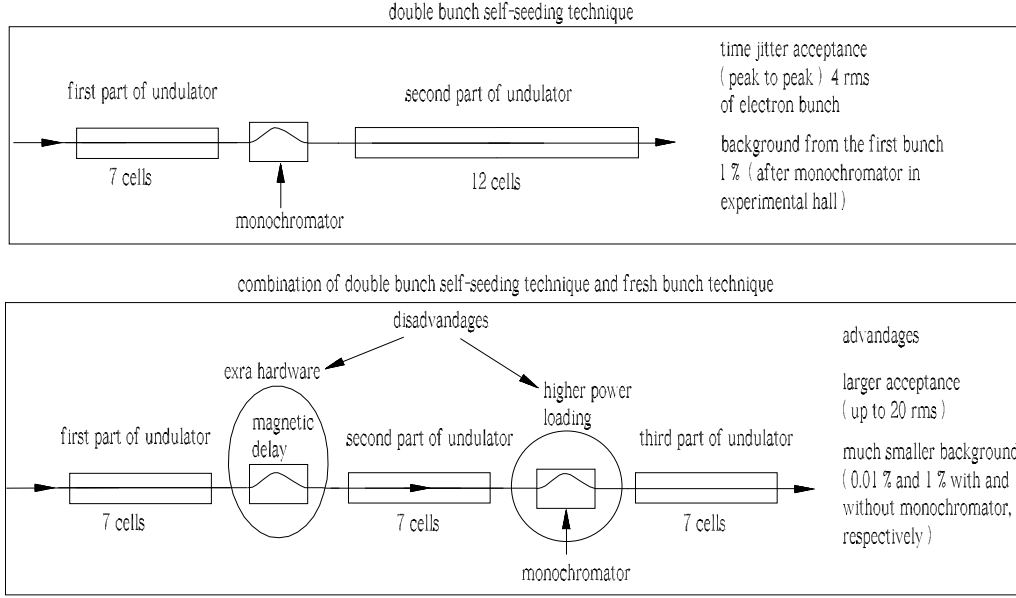


Fig. 17. Comparison of the two self-seeding schemes considered in this paper. The scheme based on the additional use of the fresh-bunch technique has two significant advantages. It is insensitive to non-ideal effects like time-jitter between two electron bunches, and presents much smaller background from the first (non monochromatic) X-ray pulse. However, in this scheme the first crystal in the monochromator operates at much more severe heat-loading conditions.

The second advantage is constituted by the fact that the background SASE radiation from the first bunch now carries much smaller power with respect to the monochromatic pulse, at variance with what happens when no fresh bunch technique is used. Note that users may also want to use an additional monochromator in the experimental hall (for example using Silicon 111 or Silicon 220). In this case, the second pulse (already monochromatized) would simply pass through without any change, and monochromatization would affect the first pulse only. In the case of a short pulse, the third undulator part only consists of 7 cells. The contribution of the first pulse will be a few per cent of the monochromatized pulse even without filtering, and would reduce to about 0.01% after filtering. Note that head-loading problems will be severe at the European XFEL (but not at LCLS) in the case of a long-pulse mode of operation. Yet, this scheme allows, in principle, for bandwidth limited pulse mode operation for 50 fs pulses too. Such mode of operation ultimately leads to an increase in peak brilliance of two orders of magnitude.

It should also be remarked, that the possibility of combining self-seeding scheme and fresh-bunch technique would be of great importance during the commissioning stage of our scheme. The inclusion of an extra chicane is not expensive and may find many other applications [15]-[19]. Moreover, it adds on to the jitter budget, and to the accuracy of the extra-path length



combination of single bunch self seeding technique and fresh bunch technique

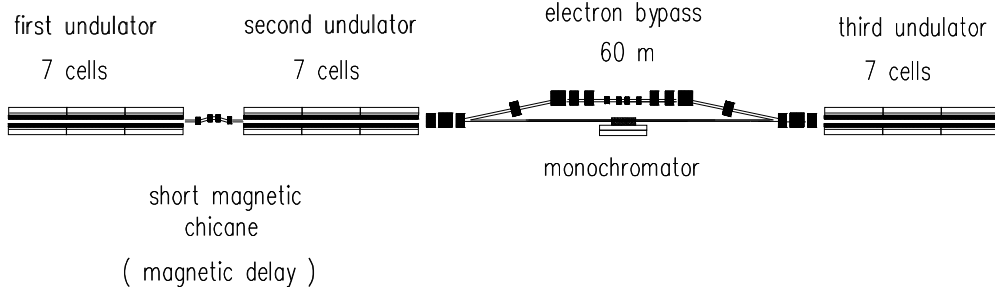


Fig. 18. Design of an undulator system for narrow bandwidth mode of operation. The method is based on a combination of single bunch self-seeding scheme and fresh bunch technique.

in the monochromator and in the pulse doubler, as one has a few orders of magnitude more input power than strictly needed. During commissioning, all non ideal effects can be reduced to a minimum and, finally, the fresh bunch scheme may be reduced to the previously discussed scheme.

It should be mentioned that the fresh bunch technique may also be combined with the single-bunch self-seeding option, as described in Fig. 18. This will allow one to work with Si(400) and Si(444) reflections. The extra-available seeding power allows for the production, at the exit of the third undulator, of bandwidth limited X-ray pulses with small level of noise contribution. This can be important for further manipulation of electron bunch and X-ray pulse, for example attempting to increase the efficiency of an XFEL by tapering.

Finally note that, when considering single-bunch self-seeding schemes, one should account for diffraction of the radiation along the 60 m free-flight between first and second undulator. Simulations show that this leads to a degradation of the effective seeding power of about a factor ten. In this case one should straightforwardly upgrade the original setup to include two more cells (from 7 to 9) in the first undulator, which we did not consider in this paper. However, increase of the total energy from the first stage of a factor ten also implies an increase of a factor ten in heat-load of the monochromator. It follows that heat loading may become an issue for the implementation of some variant (long pulse, single-bunch self-seeding in combination with fresh bunch technique) of our technique at the European

XFEL.

### 3 Feasibility study for short pulse mode of operation

Following the introduction of the proposed methods, in the present and in the following sections we report on a feasibility study performed with the help of the FEL simulation code GENESIS 1.3 [20] running on a parallel machine.

Simulations were performed in the following way: first, we calculated the three-dimensional field distribution at the exit of the first undulator, and downloaded the field file. Subsequently, we performed a Fourier transformation followed by filtering through the monochromator, by using the reflectivity curve for the specific four-bounces Bragg reflection. Finally, we performed an inverse Fourier transformation, and used the field file as seed at the entrance of the second undulator. The electron microbunching is washed out by the presence of non-zero  $R_{56}$ , and for the second undulator we used a beam file with energy and energy spread introduced by the FEL amplification process in the first undulator. The amplification process in the second undulator starts from the seed-field file. Shot noise initial condition was included. It is understood that these simulations also apply for the single bunch self seeding scheme.

#### 3.1 Two-stage scheme

##### 3.1.1 First stage

In this section we present results of numerical studies of the first stage of operation of the self-seeding setup. Parameters chosen are reported in Table 1. Fig. 19 shows a typical single-shot temporal profile of a SASE pulse, together with the average temporal structure and the electron beam profile just after the undulator. The corresponding spectra are shown in Fig. 20. Fig. 21 shows the shot-to-shot fluctuations of the SASE pulse after the exit of the first undulator. Since the first stage is in the linear regime, the radiation process obeys Guassian statistics.

Using well-known results obtained in the framework of statistical optics, we can state that the distribution of the radiation energy  $E$  after the monochromator is described rather well by the gamma probability density function  $p(E)$ :

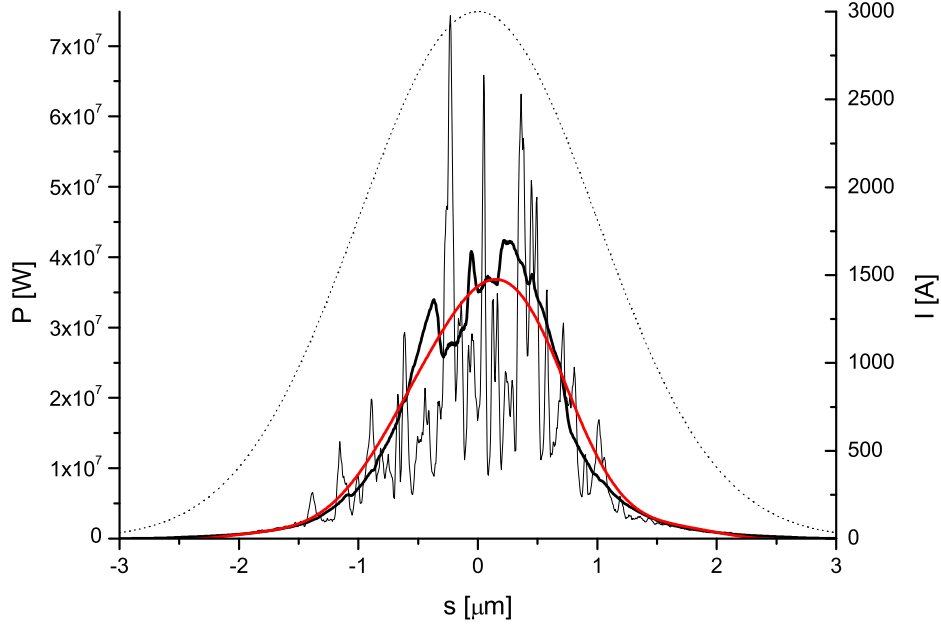


Fig. 19. Average (bold) and typical single-shot temporal structure of the SASE radiation pulse at the exit of the first undulator with a length of 42 m (7 cells). A smoothed average line is also presented. Calculations have been performed over 100 shots. The dashed line presents the corresponding distribution of the electron beam current.

Table 1

Parameters for the short pulse mode of operation used in this paper.

	Units	
Undulator period	mm	48
K parameter (rms)	-	2.516
Wavelength	nm	0.15
Energy	GeV	17.5
Charge	nC	0.025
Bunch length (rms)	μm	1.0
Normalized emittance	mm mrad	0.4
Energy spread	MeV	1.5

$$p(E) = \frac{M^M}{\Gamma(M)} \left( \frac{E}{\langle E \rangle} \right)^{M-1} \frac{1}{\langle E \rangle} \exp \left( -M \frac{E}{\langle E \rangle} \right), \quad (1)$$

where  $\Gamma(M)$  is gamma function with argument  $M$ , and

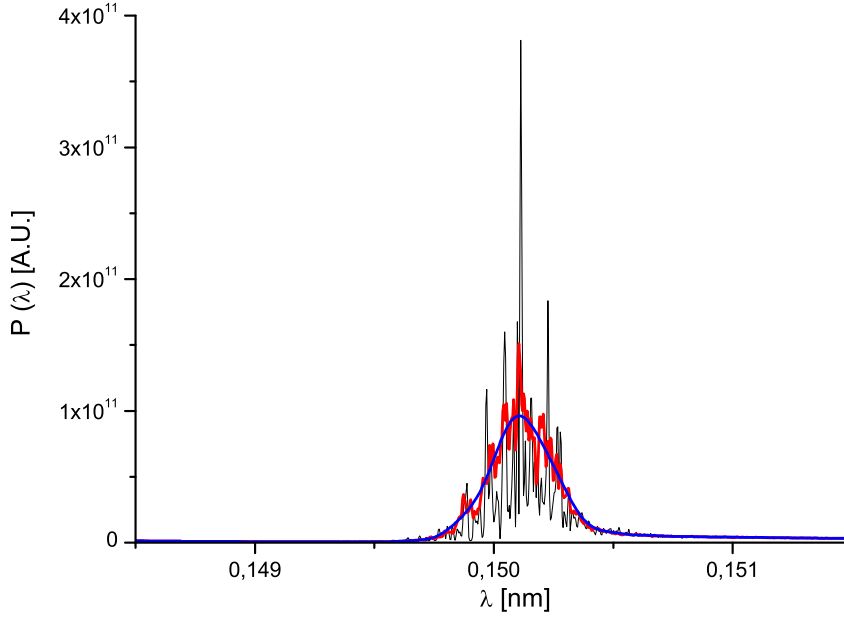


Fig. 20. Average (bold) and typical single-shot spectrum of SASE radiation at the exit of the first undulator with a length of 42 m (7 cells). A smoothed average line is also presented. Calculations have been performed over 100 shots.

$$M = \frac{1}{\sigma_E^2}, \quad (2)$$

with  $\sigma_E$  the rms energy fluctuation. This distribution provides correct values for the mean  $Z < E >$  and for the variance  $\sigma_E^2 = 1/M$ ,

$$\int_0^\infty E p(E) dE = < E >, \quad \int_0^\infty \frac{(E - < E >)^2}{< E >^2} p(E) dE = 1/M. \quad (3)$$

The parameter  $M$  can be interpreted as an average number of degrees of freedom (or modes) in the radiation pulse. We calculated  $< E >$  and  $\sigma_E^2$  from the simulation data for different reflections which yields  $M \simeq 130$ . Then,  $p(E)$  calculated according to Eq. (1) could be plotted in Fig. 22 together with the histogram of the probability density distribution of radiation, also independently obtained from the data. It is seen that it fits the gamma distribution well.

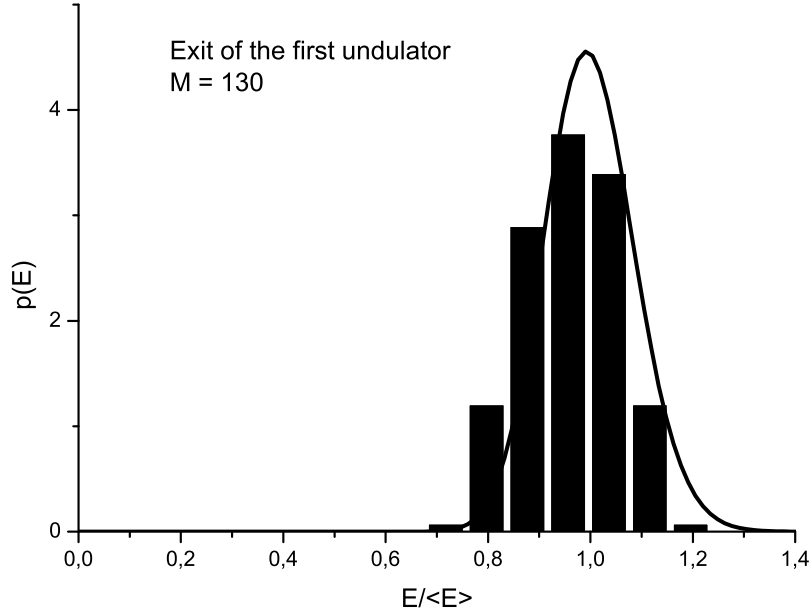


Fig. 21. Shot-to-shot fluctuations of the SASE radiation pulse at the exit of the first undulator with a length of 42 m (7 cells). Calculations have been performed over 200 shots. Here  $\langle E \rangle$  denotes the average energy. The solid curve represents the gamma distribution, Eq. (1), where the value  $M$  has been calculated from the simulation data according to Eq. (2).

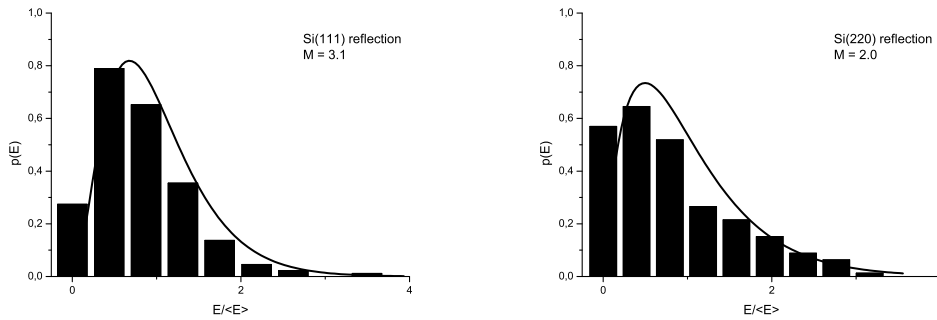


Fig. 22. Histogram of the probability density distribution  $p(E)$  of radiation energy after the four-bounce monochromator. Si(111) (left) and Si(220) (right) reflection cases. Calculations have been performed over 200 shots. Here  $\langle E \rangle$  denotes the average energy. The solid curve represents the gamma distribution, Eq. (1), where the value  $M$  has been calculated from the simulation data according to Eq. (2).

### 3.1.2 Second stage

After the first stage, radiation is monochromatized. Since the monochromator acts as a linear filter, the radiation process still obeys Gaussian statistics.

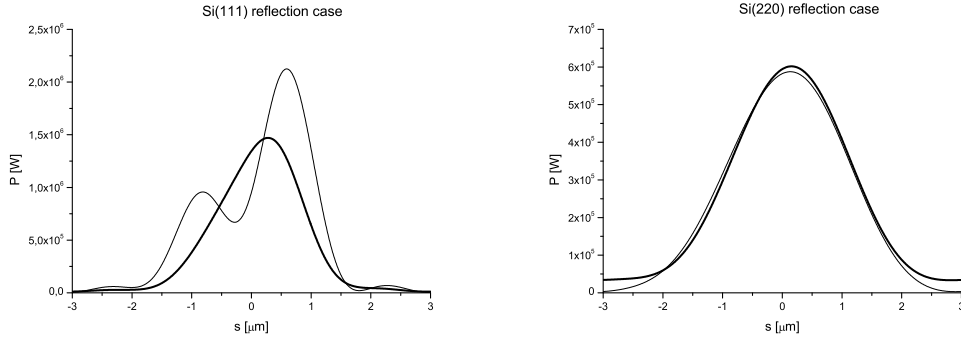


Fig. 23. Average (bold) and typical single-shot temporal structure of the radiation pulse after the four-bounce monochromator. Si(111) (left) and Si(220) (right) reflection cases.

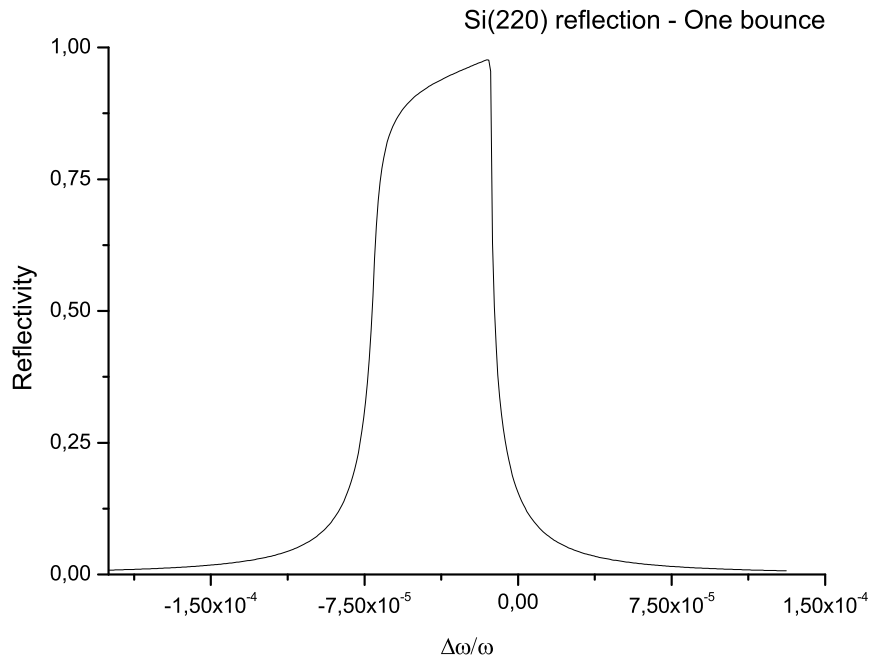


Fig. 24. Reflectivity curve for a thick absorbing crystal in Bragg geometry. Si(220) reflection of 0.15 nm X-rays. One bounce.

Fig. 22 shows the shot-to-shot fluctuations of the SASE pulse energy. Fig. 23 shows a typical single-shot temporal profile of a SASE pulse, together with the average temporal structure and the electron beam profile after a four-bounce monochromator. The reflectivity curves for the Si(220) reflection are shown in Fig. 24 and Fig. 25, for one bounce and four bounces, respectively. The reflectivity curves for the Si(111) reflection have already been shown in Fig. 12 and Fig. 13, also for one bounce and four bounces. The field profiles after different monochromators are shown in Fig. 26. These plots illustrate the properties of the seed signal for different monochromator resolutions. If

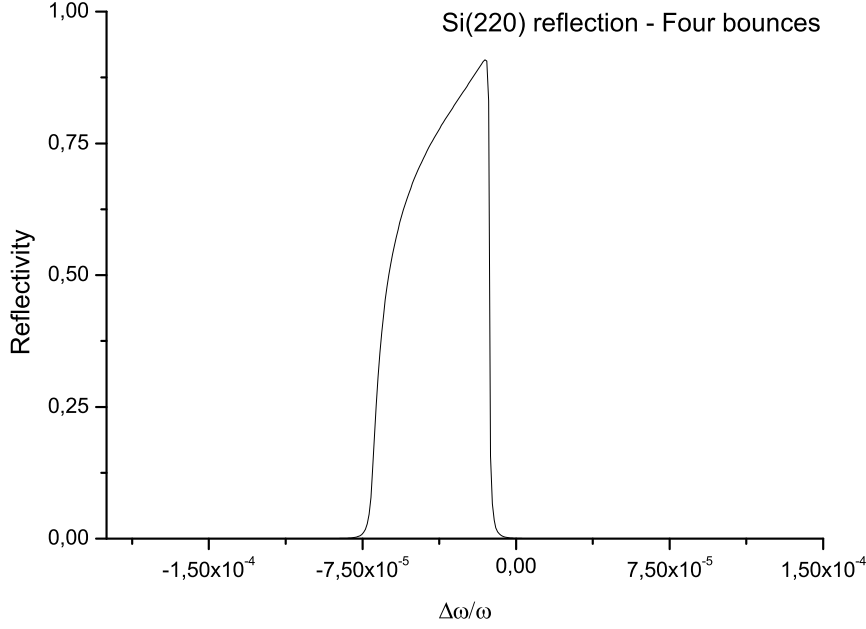


Fig. 25. Reflectivity curve for a thick absorbing crystal in Bragg geometry. Si(220) reflection of 0.15 nm X-rays. Four bounces.

the monochromator resolution is good enough, the radiation pulse is temporally stretched in such way that one only sees the characteristics of the monochromator. This is the case for Si(400), Si(440) and Si(444) reflections. The jitter acceptance is obviously linked to the FWHM width of these plots, i.e. to the temporal line width of the monochromator. Note that in Fig. 26, as everywhere in this paper, we treated the monochromator as a real filter. The effects of non-zero phase is discussed in Appendix.

Following the monochromator, we consider the outcome from the second undulator part, either using the Si(111) or the Si(220) reflection. These results constitute the output of our scheme, and demonstrate that we can obtain nearly Fourier-limited, ten-GW power level pulses of SASE radiation in the Angstrom wavelength range. The pulse energy, averaged over 100 shots, is presented as a function of the position along the second undulator in Fig. 27 for the case of the Si(111) reflection, and in Fig. 28 for the case of the Si(220) reflection. One may see that there is an optimal length of the second undulator. In both cases, saturation is expected around 70 m. We therefore consider the output after 12 cells. The shot-to-shot fluctuations of the radiation pulse after 12 cells was already studied in Fig. 22. Typical single-shot and averaged (over 200 shots) temporal structure and spectra of the radiation pulse at the undulator length of 72 m (corresponding to 12 cells) are presented in Fig. 29 and Fig. 30 for the Si(111) case, and in Fig.

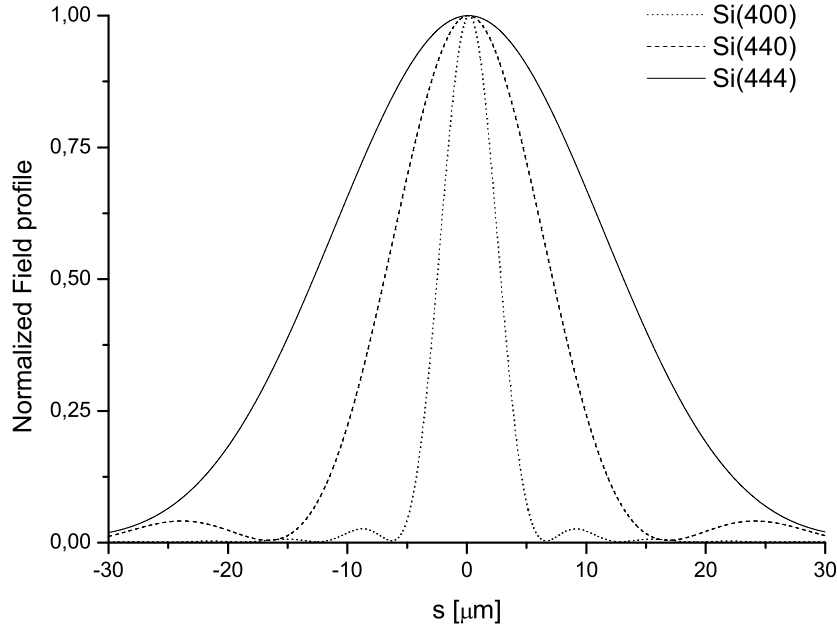


Fig. 26. Normalized field profile after the four-bounce monochromator for the short bunch case, single shot.

31 and Fig. 32 for the Si(220) case. It can be seen that the contribution of the shot noise to the total power is small. An important characteristic of the radiation is the width of the radiation spectrum. The FWHM of the radiation spectra at the undulator length of 72 m for the Silicon 111 and the Silicon 220 are about  $10^{-4}$  and  $8 \cdot 10^{-5}$  respectively, and are mainly defined by the finite pulse duration.

It is interesting to discuss the origin of the asymmetric field profile in Fig. 23 for the Si(111) reflection. Such asymmetry cannot be explained in terms of phase of the monochromator filter (which is discussed in Appendix), as the filter is considered real, in our calculations. It cannot be explained in terms of a spurious result due to finite statistics either. Therefore, we ascribe this effect to a physical phenomenon. The first stage operates in the deep linear regime. Therefore, analytical methods can be applied to describe the situation. In particular one can use the analytical solution for the initial value problem in the high-gain limit and in the frequency domain (the FEL Green's function). The growing root of the eigenvalue equation can be expanded near exact resonance. As a result, the imaginary part of the FEL Green's function includes a term proportional to the square of the detuning parameter. The asymmetry takes place due to this quadratic dependence of the imaginary part of Green's function on the frequency. Effects related to the FEL Green's function phase have been studied in [10] for both HGHG



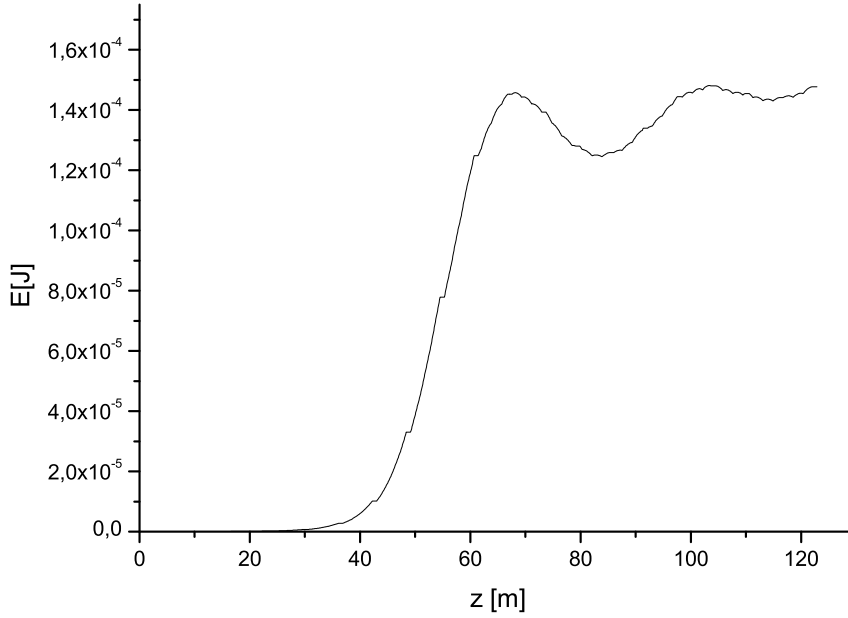


Fig. 27. Average pulse energy as a function of the position along the second undulator for the Si(111) reflection case.

and self-seeding cases. It should be added that such effect is only important when the width of the filter is comparable with the interval of spectral coherence, and can be neglected when the spectral width of the filter is a few times shorter than the spectral coherence interval. Therefore, this effect is only important for the Si(111) reflection and for the case of a short pulse, while it is much weaker in all other cases.

A typical figure of merit used to characterize the radiation from third and fourth generation light sources is the brilliance. One can estimate the foreseen brilliance for the cases discussed above by inspecting Figs. 30-32 to obtain the FWHM temporal duration and spectral width of the radiation pulses. Once the pulse duration (4 fs FWHM) and spectral width (0.008% FWHM) are calculated, knowing the number of photons per pulse ( $1.1 \cdot 10^{11}$ ) and assuming perfect transverse coherence one estimates a brilliance in the order of  $5 \cdot 10^{34} \text{ph/s/mm}^2/\text{mrad}^2/0.1\% \text{BW}$ , which is about one order of magnitude larger than the design parameter.

It is interesting to discuss the behavior of the rms pulse energy fluctuations along the undulator, which is shown in Fig. 33 and Fig. 34 for the Si(111) and for the Si(220) case respectively. As one may see, at the beginning of the undulator the fluctuations of energy per pulse apparently drop. This can be explained considering the fact that the Genesis output consists of the total power integrated over the full grid up to an artificial boundary, i.e.

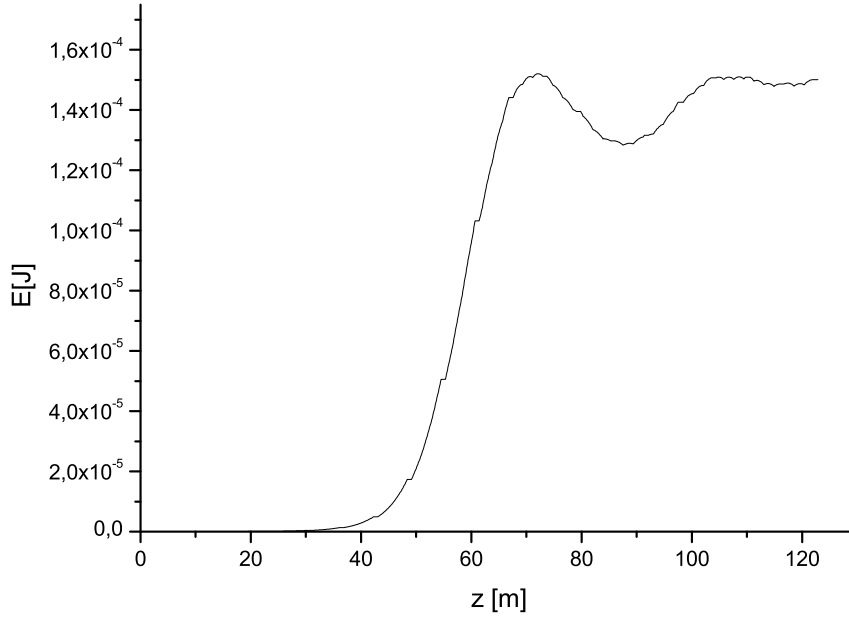


Fig. 28. Average pulse energy as a function of the position along the second undulator for the Si(220) reflection case.

there is no spectral selection. Therefore, Fig. 33 includes a relatively large spontaneous emission background, which has a much larger spectral width with respect to the amplification bandwidth and which fluctuates negligibly from shot to shot. Since there is a long lethargy of the seeded radiation at the beginning of the FEL amplifier, one observes an apparent decrease of fluctuations. Then, when lethargy ends, the seed pulse gets amplified and fluctuations effectively return to the same level as after monochromator<sup>4</sup>. The energy fluctuations are drastically reduced when the FEL amplifier operates in the nonlinear regime. The minimal value of the fluctuations<sup>5</sup>, around 10%, occurs at the undulator length of 72 m (12 cells).

<sup>4</sup> Actually fluctuations return to a slightly higher level compared to that after the monochromator. This can be explained considering the fact that we deal with a parametric amplifier, where the properties of the active medium, i.e. the electron beam, depend on time. The duration of the electron bunch is shorter compare to the duration of the seed pulse. Therefore, the amplified pulse has effectively higher coherence compared to the full radiation pulse after the monochromator, hence the higher fluctuation level.

<sup>5</sup> The oscillations of the energy fluctuations after this point are connected with the growth of spikes in the nonlinear medium, since we have taken into account the shot noise in the electron beam. The spectrum gets broader due to such spikes growth. The total power can even increase, while the maximum value of the spectral density decreases.

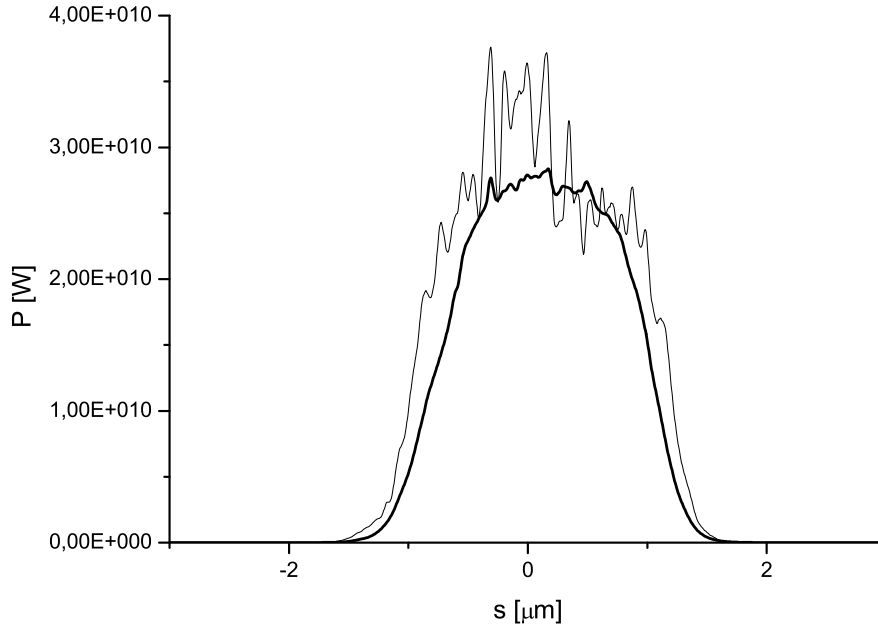


Fig. 29. Average (bold) and typical single-shot temporal structure of the radiation pulse at the second undulator length of 72 m (12 cells) for the Si(111) reflection case.

Finally, let us briefly analyze the heat loading problem. For the short pulse mode of operation and for the European XFEL case we have an average power of 5 mW (150 nJ  $\times$  3000 pulses/train  $\times$  10 trains/s). This corresponds to a normal incident power density<sup>6</sup> of 2W/mm<sup>2</sup> at the position of the monochromator located in baseline undulator, Fig. 6. For the double bunch scheme, this number should be increased of a factor two, up to 4W/mm<sup>2</sup>. This is more than two orders of magnitude smaller compared with the power at monochromators of third generation synchrotron sources (200W/mm<sup>2</sup>). The problem of heat loading obviously does not exist at all for LCLS, due to the much lower repetition rate, and all our results can be applied for LCLS without any limitations concerning heat loading of the monochromator.

<sup>6</sup> We consider a transverse rms dimension of the bunch of about 20 $\mu$ m. Assuming, with some approximation, that radiation is distributed as the electron bunch, we obtain an area of  $2.4 \cdot 10^{-3}$ mm<sup>2</sup>.

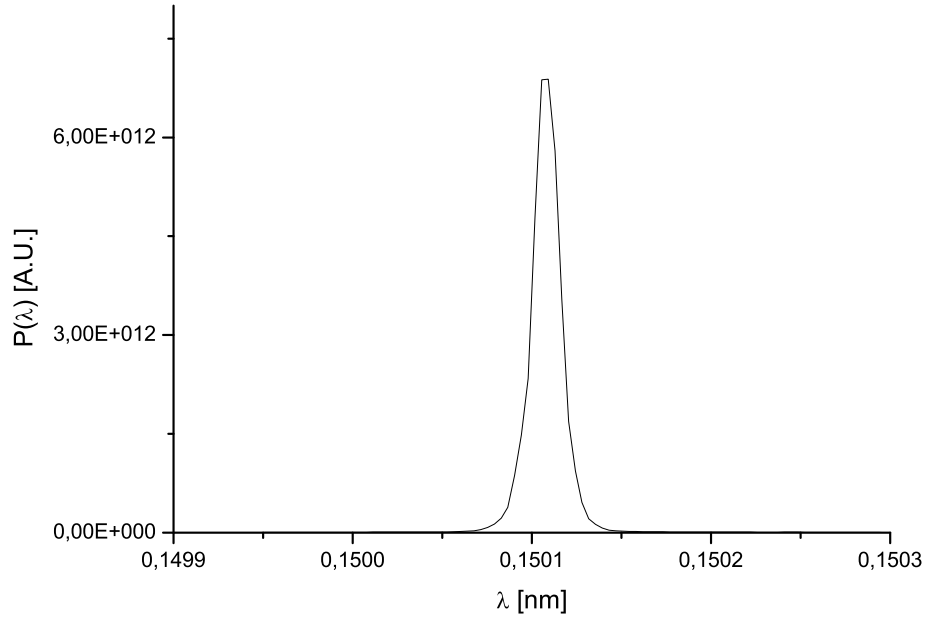


Fig. 30. Averaged spectrum of radiation at the second undulator length of 72 m (12 cells) for the Si(111) reflection case.

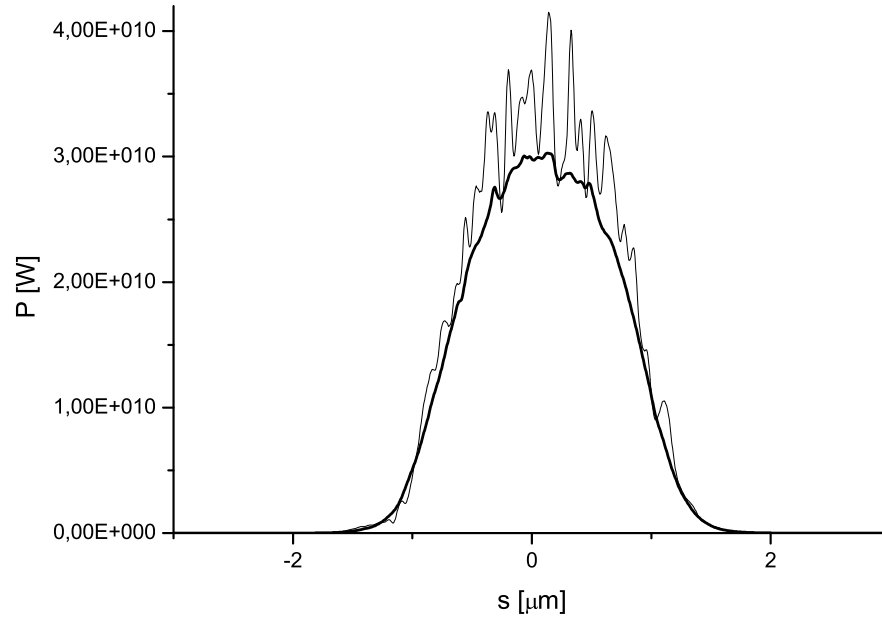


Fig. 31. Average (bold) and typical single-shot temporal structure of the radiation pulse at the second undulator length of 72 m (12 cells) for the Si(220) reflection case.

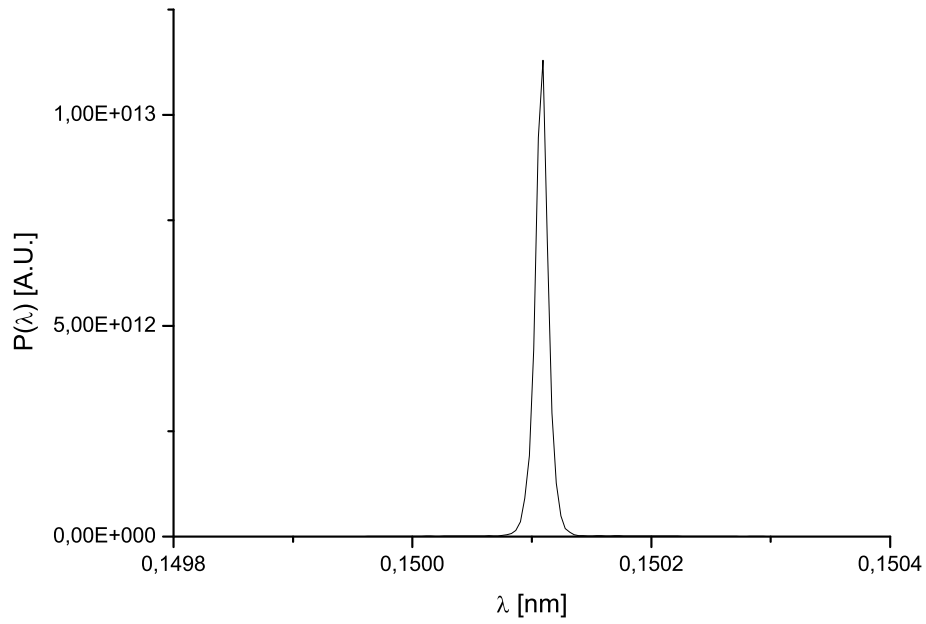


Fig. 32. Averaged spectrum of radiation at the second undulator length of 72 m (12 cells) for the Si(220) reflection case.

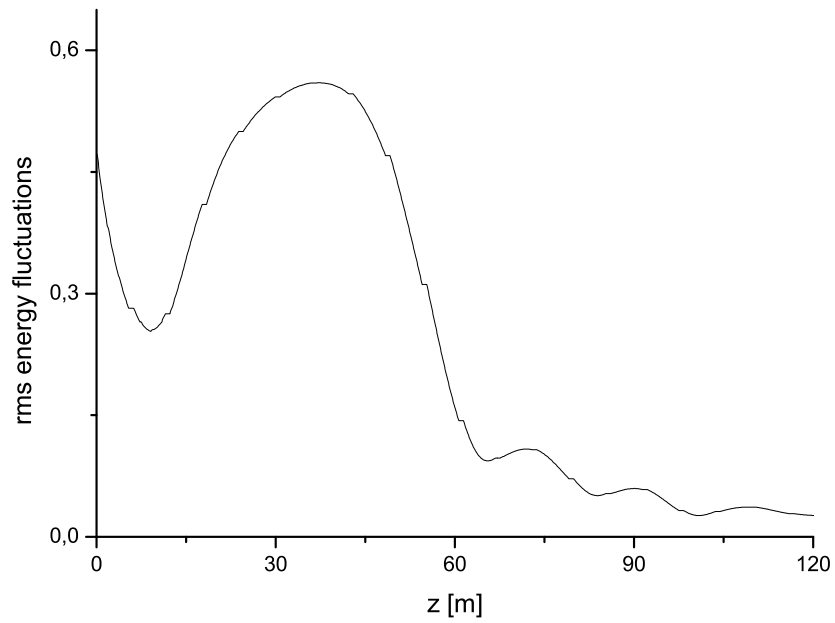


Fig. 33. RMS pulse energy fluctuations along the second undulator for the Si(111) reflection case.

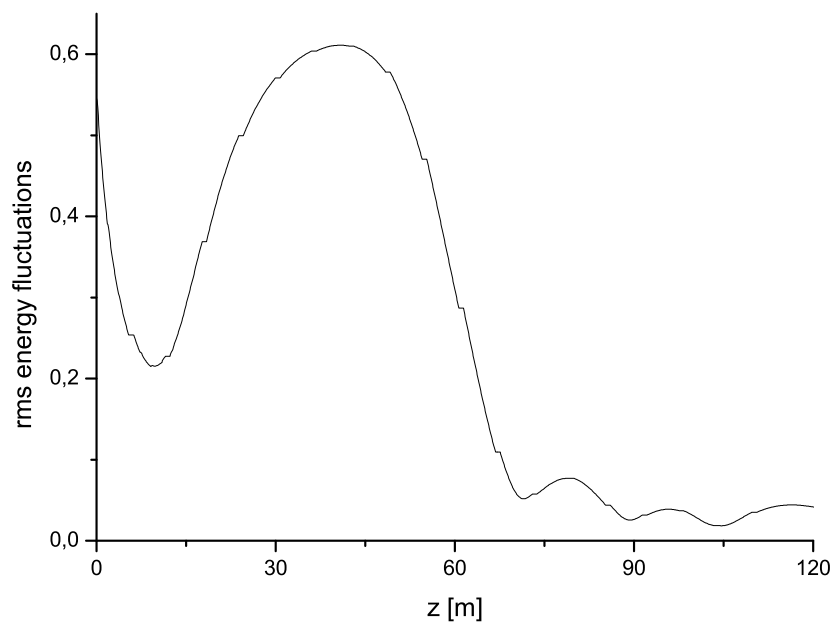


Fig. 34. RMS pulse energy fluctuations along the second undulator for the Si(220) reflection case.

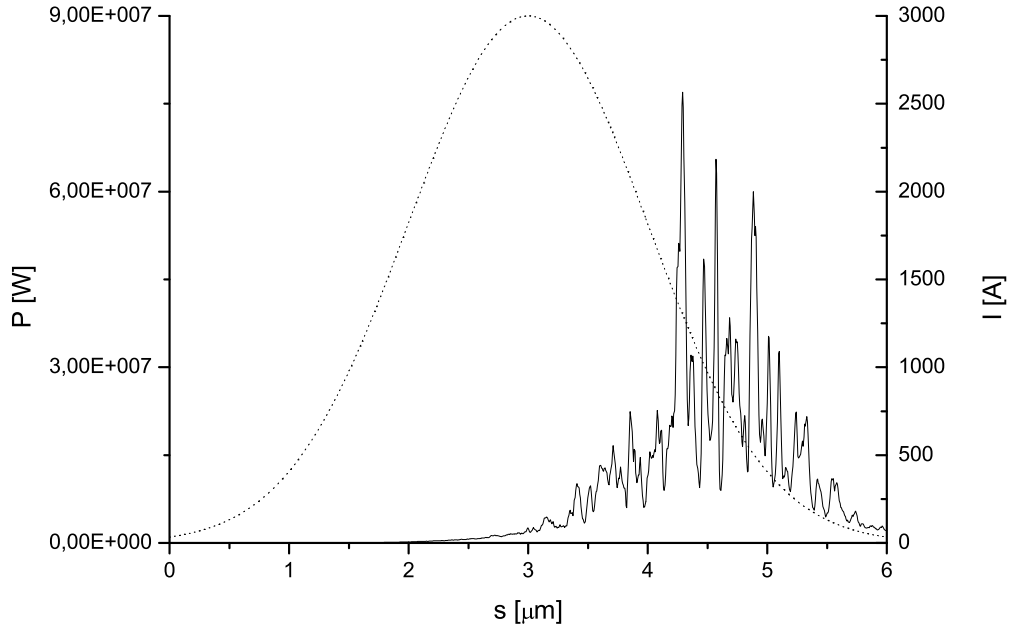


Fig. 35. Short pulse mode operation, combination of self-seeding and fresh bunch techniques. Power distribution after the first undulator part (7 cells) and the magnetic delay. Radiation is used as input for the second undulator part (7 cells).

### 3.2 *Three-stage scheme: combination of self-seeding scheme and fresh bunch technique*

Combination of our self-seeding scheme with a fresh bunch technique has been schematically illustrated in Figs. 14-16. The first undulator part is identical as before. However, now, between first and second part of the undulator a magnetic chicane is introduced, which washes out the electron beam microbunching and provides a relative delay between electron beam and radiation. Then, the head of the electron bunch is seeded by the radiation from the first undulator part and saturates faster in the second part of the undulator.

The first stage is 7-cells long, and the properties of the radiation at its exit have already been illustrated in Fig. 19 and in Fig. 20. In Fig. 35 we illustrate the input power at the second stage. Fig. 36 shows the output power from the second stage, which is 7-cells long, while the correspondent spectrum is given in Fig. 36. Following the second part of the undulator, the electron bunch enters the self-seeding stage, where radiation is monochromatized. In Fig. 38 and Fig. 39 we show the reflectivity curves for a thick absorbing crystal in the case of the Si(400) reflection, for a single bounce and for four bounces. With the help of the fresh bunch technique we now can use, for

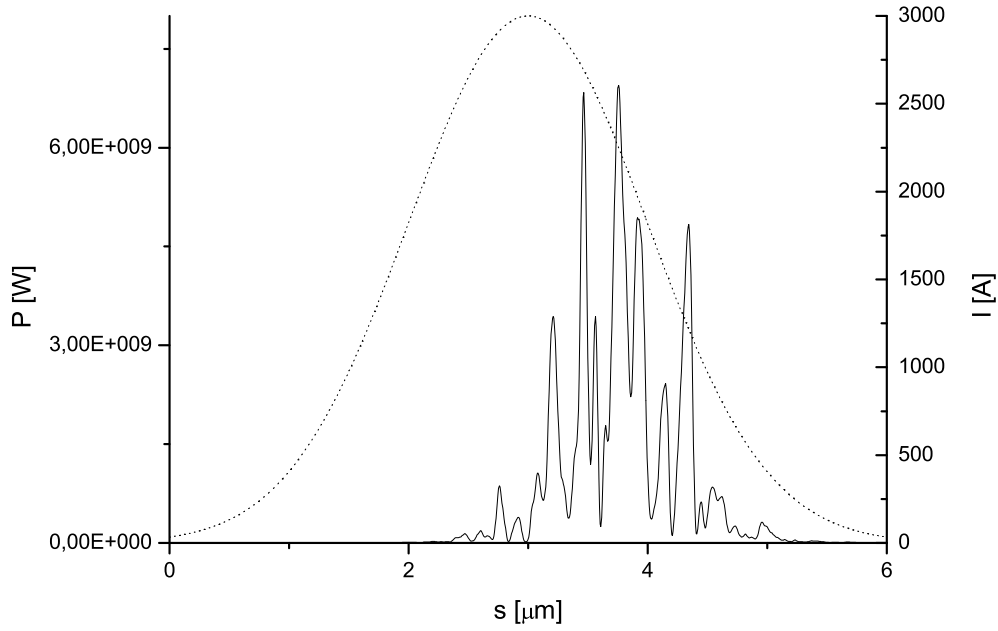


Fig. 36. Short pulse mode operation, combination of self-seeding and fresh bunch techniques. Output power at the end of the second stage, 7 cells long (42 m).

monochromatization purposes, reflections like Si(400), Si(440) and Si(444). The field profiles using these kind of reflections have already been shown in Fig. 26. As noted before, the jitter acceptance is obviously linked to the FWHM width of these plots, i.e. to the temporal line width of the monochromator. Since Si(400), Si(440) and Si(444) reflections are associated to a smaller bandwidth, one can take advantage of an increased jitter acceptance, which practically cancels the background from the first electron bunch for the double bunch scheme. The third undulator part follows, where the fresh part of the bunch is seeded by the monochromatized radiation. Output power and spectrum at the end of the 8-cells setup are shown in Fig. 40 and Fig. 41 respectively. From Fig. 41 one can see that radiation is nearly fully longitudinally coherent.

As regards heat-loading issues, from Fig. 36 follows that one has an average power of about 3 GW, which is two order of magnitude larger than the 30 MW considered in the previous two-stage scheme. Since the pulse is twice shorter we have a power density of about  $200 \text{ W/mm}^2$ , still within an acceptable value.



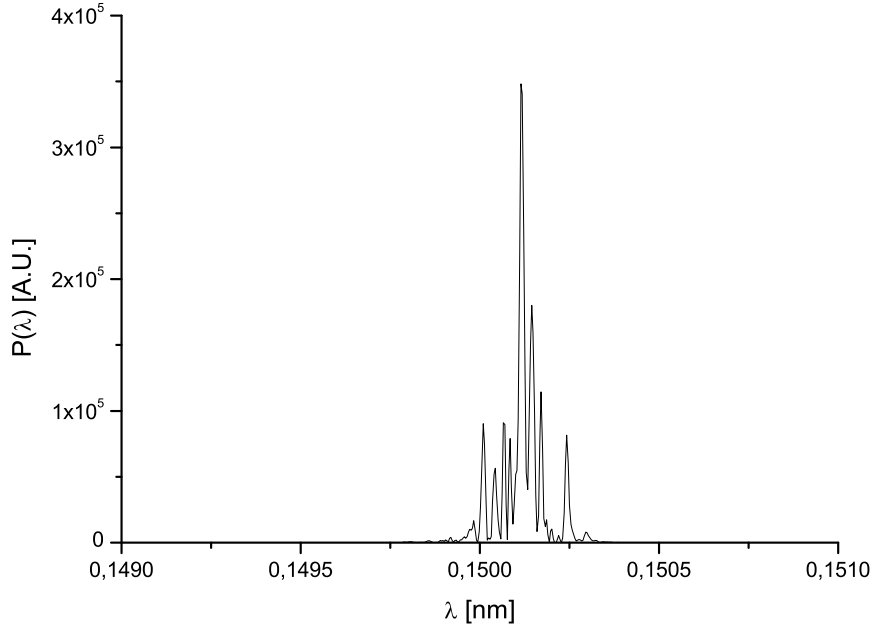


Fig. 37. Short pulse mode operation, combination of self-seeding and fresh bunch techniques. Output spectrum at the end of the second stage, 7 cells long (42 m).

#### 4 Feasibility study for the long pulse mode of operation

We also performed a feasibility study for the long-pulse mode of operation. We assume that parameters in Table 1 are still valid, except for a ten times larger charge (0.25 nC) and a ten times longer rms bunch length (10  $\mu\text{m}$ ). We considered both the two-stage scheme and a combination of self-seeding and fresh-bunch techniques. In the following we will discuss outcomes from a single-shot simulation.

##### 4.1 Two stage-scheme

The first stage is 7-cells long. First we consider the Si(220) reflection case. The power after the first undulator part and after monochromatization is shown in Fig. 42. The output of our scheme is shown in Fig. 43, illustrating the power after the second undulator part, and in Fig. 44, illustrating the spectrum. The presence of a few longitudinal modes can be guessed by inspection of Fig. 43 and Fig. 44.

Subsequently, we analyze the case for the Si(400) reflection. The power after the first undulator part and after monochromatization is shown in Fig.

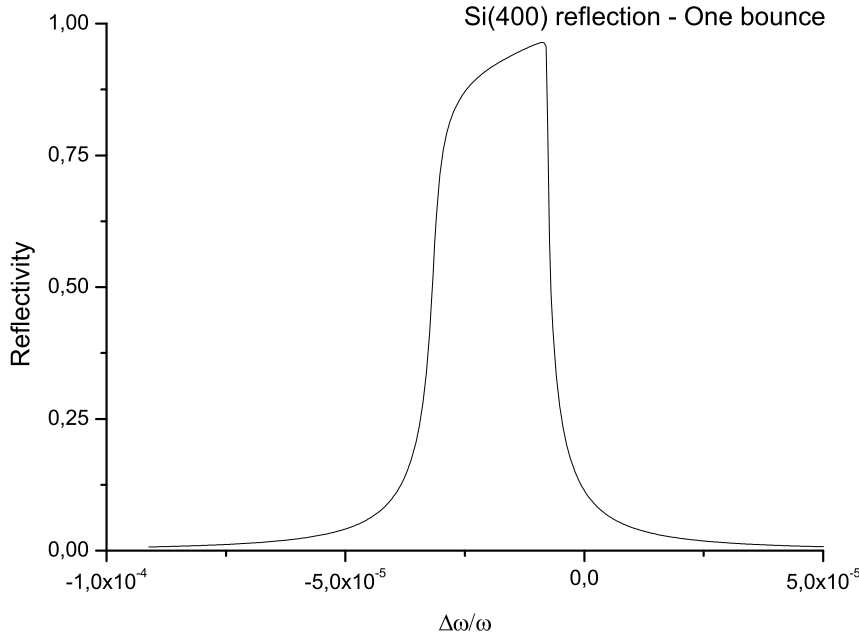


Fig. 38. Reflectivity curve for a thick absorbing crystal in Bragg geometry. Si(400) reflection of 0.15 nm X-rays. One bounce.

45. The final output is shown in Fig. 46, illustrating the power after the second undulator part, and in Fig. 47, illustrating the spectrum. The narrower monochromator bandwidth results in almost longitudinally coherent radiation, as it can be guessed by inspection of Fig. 46 and Fig. 47.

Concerning heat-loading problems, it should be noted that the power density in this case increases of an order of magnitude compared with the two stage, short pulse mode of operation (as the rms duration also increases of that magnitude). This results in an average power density of about 40W/mm<sup>2</sup>, which is well manageable for silicon crystals.

#### 4.2 *Three-stage scheme: combination of self-seeding scheme with fresh bunch technique*

We finally considered a three-stage scheme, combining the self-seeding scheme with a fresh-bunch technique. The first stage is 7-cells long. Fig. 48 and Fig. 49 illustrate power and spectrum at the exit of second undulator part, before the monochromator, which is 7-cells long too. The monochromatization is performed using the Si(444) reflection. The reflectivity curves relative to this case are shown in Fig. 50 and Fig. 51 for one and four bounces respectively. Fig. 52 shows a typical single-shot power profile

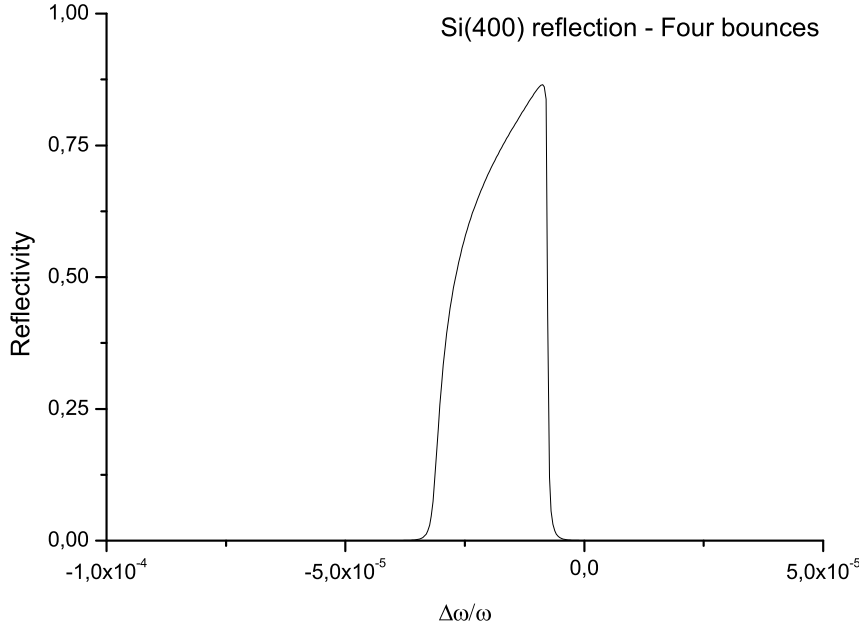


Fig. 39. Reflectivity curve for a thick absorbing crystal in Bragg geometry. Si(400) reflection of 0.15 nm X-rays. Four bounces.

after monochromatization. Finally, Fig. 53 and Fig. 54 show the output of our scheme, respectively in terms of power and spectrum.

It should be noted, that in this case the power density on the monochromator is about  $2\text{kW}/\text{mm}^2$  which is ten times more than the typical heat load of monochromators in third generation sources. To solve such problem, we suggest to use the first two Bragg reflectors as a high heat-load premonochromator, which drastically reduces the heat load from the actual high resolution monochromator, constituted by the third and the fourth crystal [7]. In the premonochromator one may take advantage of diamond crystal plates about  $100\mu\text{m}$  thick and of the Bragg reflection C(004). Considering a perfect crystal, it will reflect 99% of the incident X-rays. Only 5% of the off-band radiation will be absorbed, while the rest will pass through. The absorbed power is thus 20 times less than incident power, resulting in an absorbed power density of about  $100\text{W}/\text{mm}^2$ , of the same magnitude of the heat load of monochromators in third generation sources, Fig. 55.

Similarly to what has been done for the short-pulse case, it is interesting to estimate the brilliance in the long-pulse case as well. With the help of Fig. 53 and Fig. 54 we obtain an additional increase of about one order of magnitude with respect to the short-bunch case (i.e. two orders of magnitude with respect to the baseline design) due to the narrower spectral width of the Si(444) reflection, yielding a peak brilliance of the order of

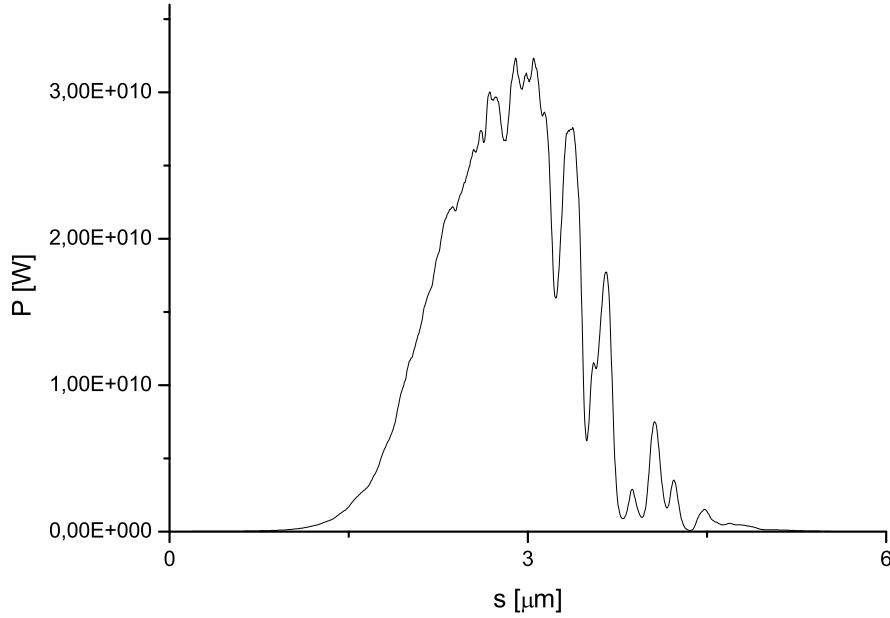


Fig. 40. Short pulse mode operation, combination of self-seeding and fresh bunch techniques. Four bounce monochromator, Si(400) reflection. Output power at the end of the third stage, 8 cells long (53 m).

$$5 \cdot 10^{35} \text{ph/s/mm}^2/\text{mrad}^2/0.1\% \text{BW}.$$

## 5 Conclusions

In this paper we studied methods to reduce the line width of a SASE X-ray FEL. One is based on the single bunch self-seeding scheme. This method consists of two undulators with an X-ray crystal monochromator located between them. The realization of this single bunch self-seeding scheme for XFELs requires a 60 m-long electron bypass to compensate for the X-ray path delay introduced by the monochromator. This scheme is not compatible with the baseline mode of operation of XFEL facilities, and as a result it cannot be implemented from the very beginning of the operation stage. In this paper we propose a method to get around this obstacle by using a double bunch scheme where radiation from the first bunch seeds the second. This scheme overcomes the bypass problem, although research and development is required to develop a suitable laser-pulse doubler. Combination with a fresh-bunch technique is discussed too, and will be particularly important during the commissioning phase. We discussed both short and long-pulse scenarios, and presented a feasibility study which can be applied to all the

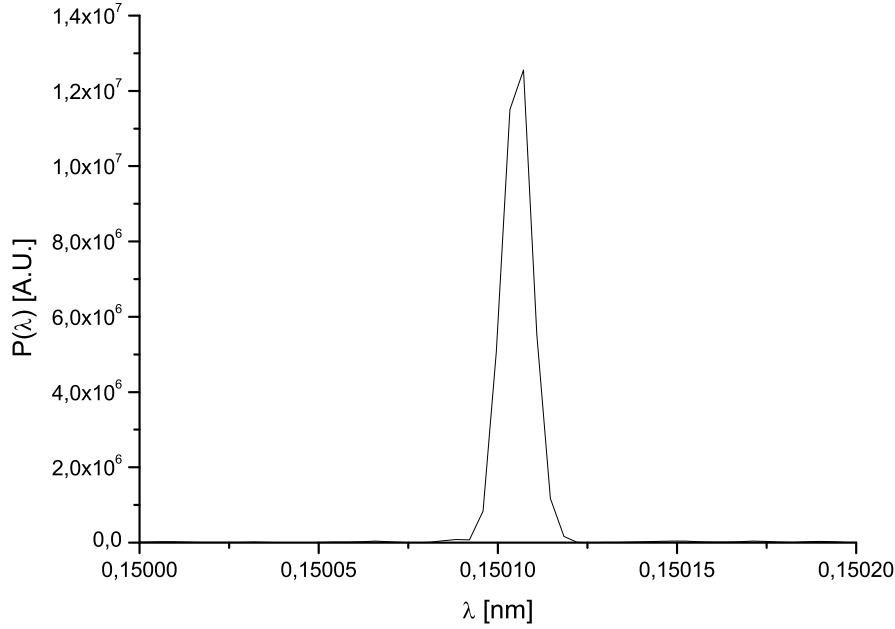


Fig. 41. Short pulse mode operation, combination of self-seeding and fresh bunch techniques. Four bounce monochromator, Si(400) reflection. Output spectrum at the end of the third stage, 8 cells long (53 m).

considered techniques.

An estimation of the peak brightness of the pulses produced with our methods shows an increase up to  $5 \cdot 10^{35}$  ph/s/mm<sup>2</sup>/mrad<sup>2</sup>/0.1%BW, i.e. two orders of magnitude with respect to the baseline parameters. However, it should be noted that the brilliance may not be an adequate figure of merit to consider when we deal with fully longitudinally and transversely coherent x-ray pulses with a duration of 4 – 40 fs (respectively short pulse and long pulse mode of operation), energy per pulse in the order of 0.1 – 1 mJ, with shot-to-shot energy fluctuations within 10% and time jitter of about 50 fs (according to the LCLS results). These parameters are near to those usually reported for high-power fs laser systems, only in the x-ray regime.

Finally, it should be remarked that the self-seeding based on a double bunch presented in this paper can be implemented without disturbing the baseline mode of operation of the XFEL facility. This study is useful for the European XFEL, as well as for other present or future XFEL facilities.

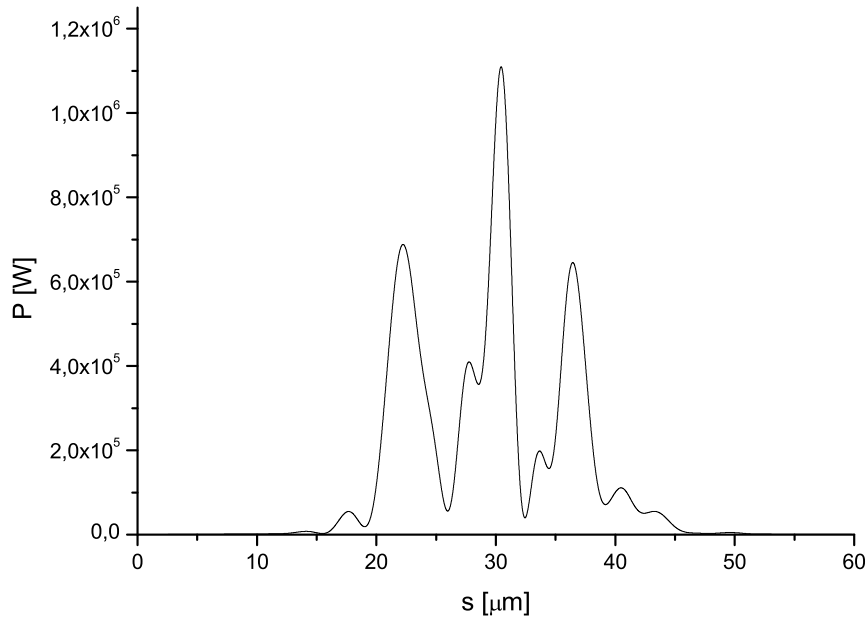


Fig. 42. Long pulse mode of operation. Power after four-bounce monochromator, Si(220) reflection. Radiation is used as input for the second undulator part.

## 6 Acknowledgements

We are grateful to Massimo Altarelli, Reinhard Brinkmann, Serguei Molodtsov and Edgar Weckert for their support and their interest during the compilation of this work.

## References

- [1] M. Altarelli, et al. (Eds.) XFEL, The European X-ray Free-Electron Laser, Technical Design Report, DESY 2006-097, Hamburg (2006).
- [2] J. Arthur et al. (Eds.) Linac Coherent Light Source (LCLS). Conceptual Design Report, SLAC-R593, Stanford (2002) (See also <http://www-ssrl.slac.stanford.edu/lcls/cdr>).
- [3] P. Emma, First lasing of the LCLS X-ray FEL at 1.5 Å, in Proceedings of PAC09, Vancouver, to be published in <http://accelconf.web.cern.ch/AccelConf/> (2009).
- [4] Y. Ding et al., Phys. Rev. Lett. 102, 254801 (2009).
- [5] T. Tanaka et al. (Eds.) Spring-8 Compact SASE Source Conceptual Design report, Kouto (2005) (See also <http://www-xfel.spring8.or.jp/SCSSCDR.pdf>)

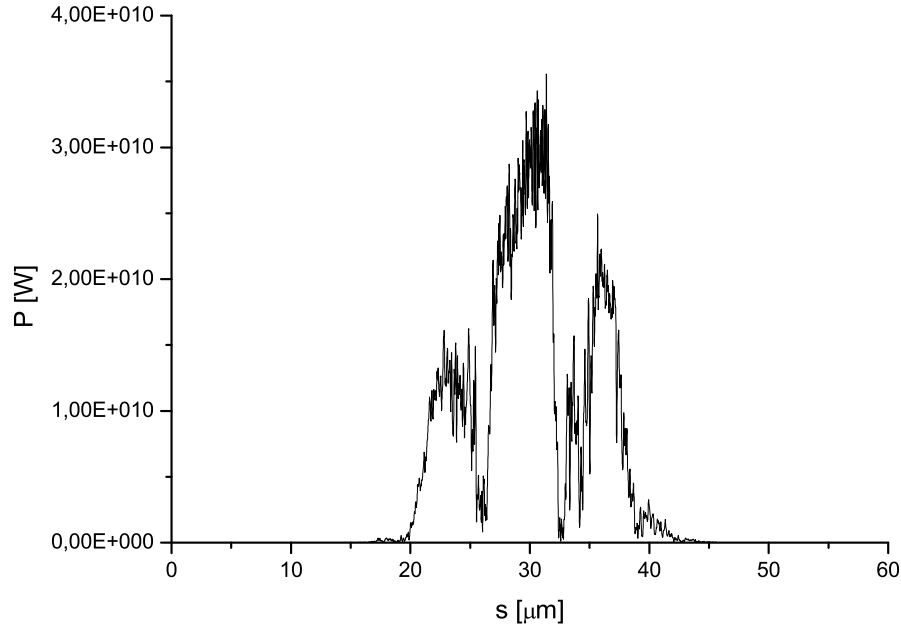


Fig. 43. Long pulse mode of operation, Si(220) reflection. Power at exit of the second undulator, with a length of 72 m (12 cells).

- [6] J. Feldhaus et al., Optics. Comm. 140, 341 (1997).
- [7] E. Saldin, E. Schneidmiller, Yu. Shvyd'ko and M. Yurkov, NIM A 475 357 (2001).
- [8] E. Saldin, E. Schneidmiller and M. Yurkov, NIM A 445 178 (2000).
- [9] R. Treusch, W. Brefeld, J. Feldhaus and U Hahn, Ann. report 2001 "The seeding project for the FEL in TTF phase II" (2001).
- [10] A. Marinelli et al., Comparison of HGHG and Self Seeded Scheme for the Production of Narrow Bandwidth FEL Radiation, Proceedings of FEL 2008, MOPPH009, Gyeongju (2008).
- [11] O. Grimm, K. Klose and S. Schreiber, Double-pulse Generation with the FLASH Injector Laser for Pump-Probe Experiments, Proceedings of EPAC 2006, THPCH150, Edimburgh (2006).
- [12] I. Ben-Zvi and L.H. Yu, Nucl. Instr. and Meth. A 393, 96 (1997).
- [13] E. Saldin, E. Schneidmiller and M. Yurkov, Opt. Commun. 212, 377 (2002).
- [14] E. Saldin, E. Schneidmiller and M. Yurkov, Opt. Commun., 239, 161 (2004).
- [15] G. Geloni, V. Kocharyan and E. Saldin, "Scheme for femtosecond-resolution pump-probe experiments at XFELs with two-color ten GW-level X-ray pulses", DESY 10-004 (2010).
- [16] G. Geloni, V. Kocharyan and E. Saldin, "The potential for extending the spectral range accessible to the European XFEL down to 0.05 nm",

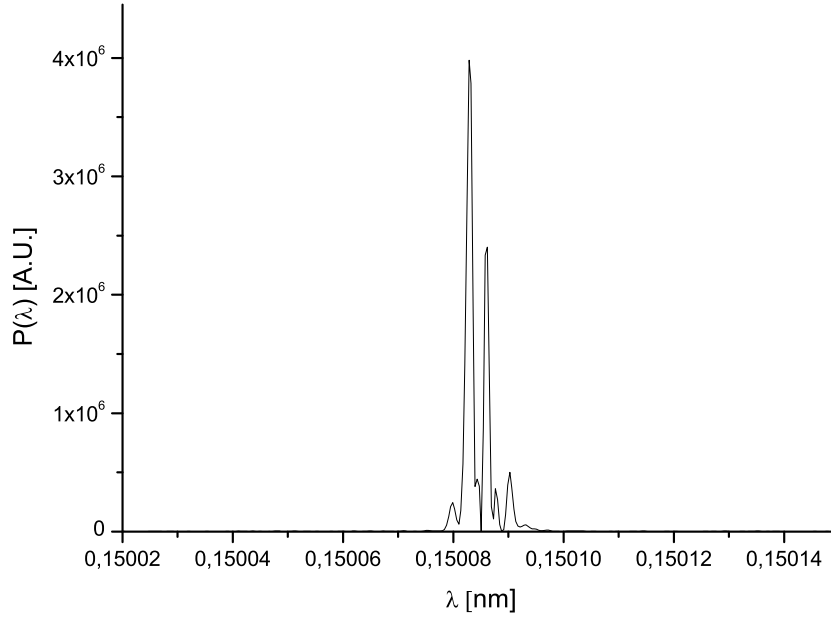


Fig. 44. Long pulse mode of operation, Si(220) reflection. Spectrum at exit of the second undulator, with a length of 72 m (12 cells).

- DESY 10-005 (2010).
- [17] G. Geloni, V. Kocharyan and E. Saldin, "Scheme for simultaneous generation of three-color ten GW-level X-ray pulses from baseline XFEL undulator and multi-user distribution system for XFEL laboratory", DESY 10-006 (2010).
  - [18] G. Geloni, V. Kocharyan and E. Saldin, "Control of the amplification process in baseline XFEL undulator with mechanical SASE switchers", DESY 10-010 (2010).
  - [19] G. Geloni, V. Kocharyan and E. Saldin, "Ultrafast X-ray pulse measurement method", DESY 10-008 (2010).
  - [20] S Reiche et al., Nucl. Instr. and Meth. A 429, 243 (1999).
  - [21] A. Authier, Dynamical Theory of X-ray diffraction, Oxford University press (2001).

### **Appendix: Influence of phase variation of X-ray waves along the reflectivity curve in Bragg geometry on the temporal profile of the seed X-ray pulse**

In this Appendix we investigate the effects of the monochromator phase on the temporal shape of the radiation pulse. In fact, up to now we assumed that the monochromator is composed of real filters, while in reality these filters include a phase. Here we show that the effects



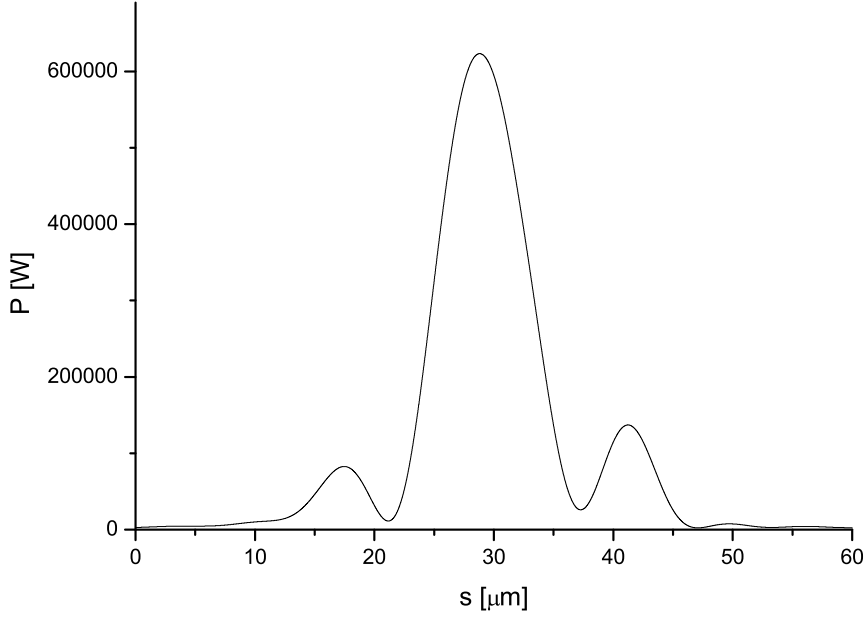


Fig. 45. Long pulse mode of operation. Power after the four-bounce monochromator, Si(400) reflection. Radiation is used as input for the second undulator part.

of such pahse is negligible. In particular, we will concentrate on the Si(400) reflection. In general, according to the dynamical theory of X-ray diffraction, the phase  $\Phi(\eta)$  and amplitude  $Z(\eta)$  introduced by a one-bounce reflection on any crystal, neglecting absorption, are given by [21]:

$$Z(\eta) = \left| \eta \pm \sqrt{\eta^2 - 1} \right| \quad (4)$$

$$\Phi(\eta) = \arg \left[ -\eta + \sqrt{\eta^2 - 1} \right] . \quad (5)$$

Here the positive or negative sign in Eq. (4) should be taken such that  $Z < 1$ . In literature  $\eta$  is the deviation parameter. If absorption is neglected as in our case, such parameter varies from  $-1$  to  $+1$  when the reflectivity is 100%. Multiplication by the bandwidth  $\Delta\omega_{nkl}/\omega$ , which depends on the reflection, yields the reflectivity curve and the phase as a function of the deviation from the center of reflectivity curve,  $\Delta\omega/\omega = \eta\Delta\omega_{nkl}/\omega$ . Thus, in our case we can say that  $\eta$  represents a reduced frequency deviation.

Starting with the reflectivity curves in Fig. 38 we matched the centers with  $\eta = 0$ , and the FWHM with  $\eta = \pm 1$ . As a result we fixed the phase change along the curve according to Eq. (5). Then, for a four-bounce

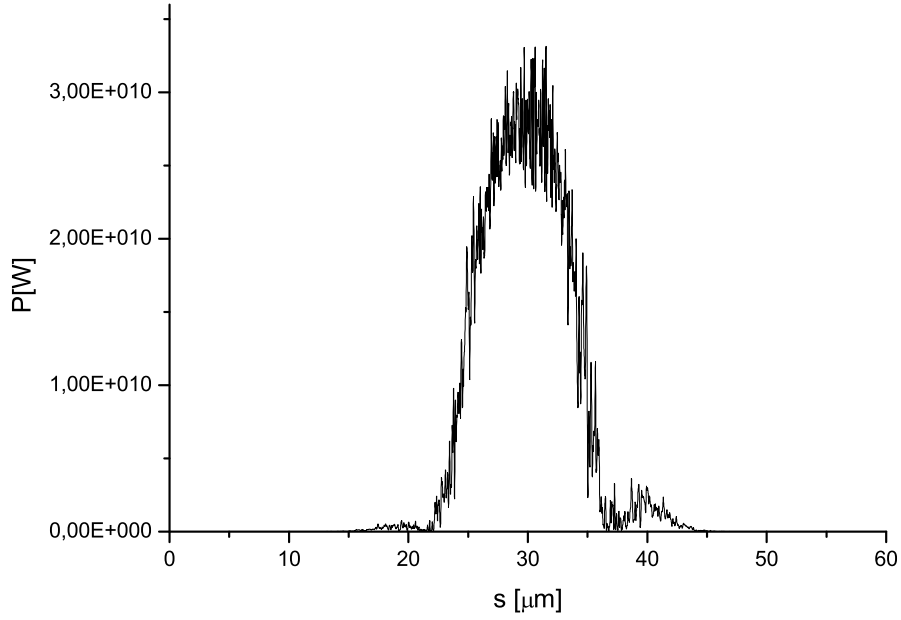


Fig. 46. Long pulse mode of operation, Si(400) reflection. Power at the exit of the second undulator, with a length of 72 m (12 cells).

reflection one needs to multiply the phase by a factor four. Now amplitude and phase are known, and we can calculate the temporal pulse profile by taking the Fourier Transform of the complex monochromator line. By this we neglect effects of absorption on the phase, which are anyway small. A comparison of the results obtained with and without phase is shown in Fig. 56. The linear component of the phase is responsible for a temporal shift, and non-linear components modify the result in a way which may be taken into account in more detailed studies. We conclude that for the purpose of giving a feasibility study of our technique it is sufficient to account for the real part of the filter line only.

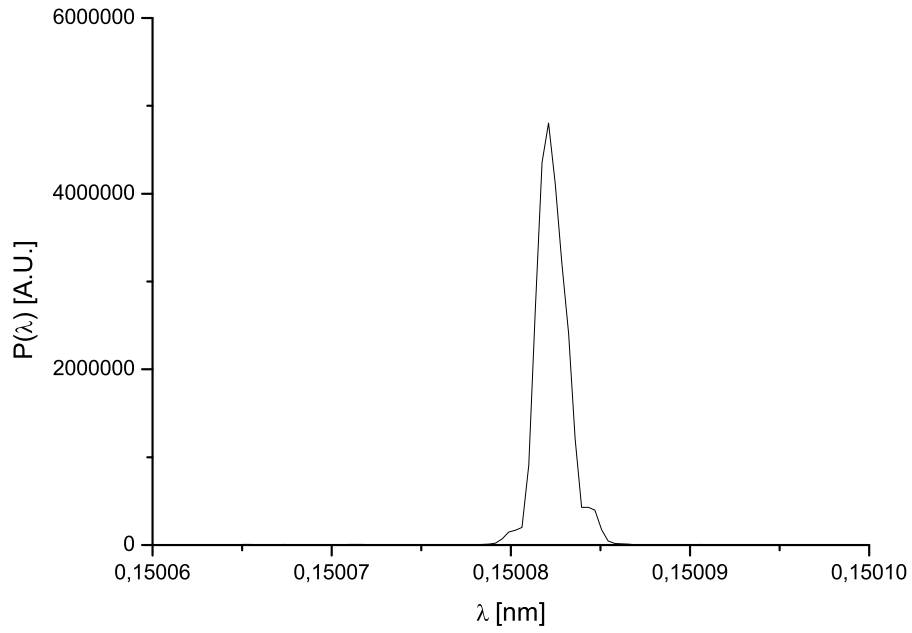


Fig. 47. Long pulse mode of operation, Si(400) reflection. Spectrum at the exit of the second undulator, with a length of 72 m (12 cells).

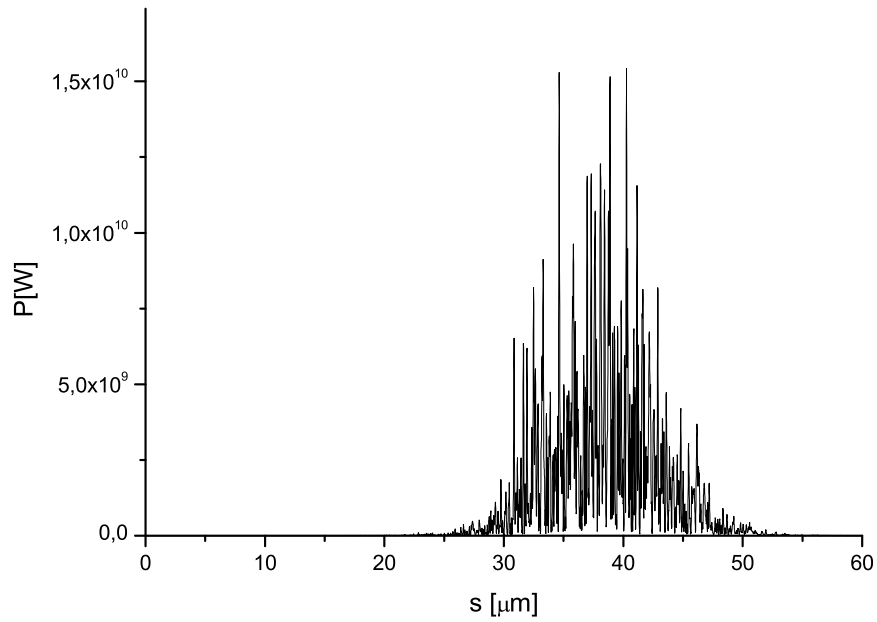


Fig. 48. Long pulse mode operation. Combination of self-seeding and fresh bunch techniques. Power at end of the second stage, 7cells long (42 m).

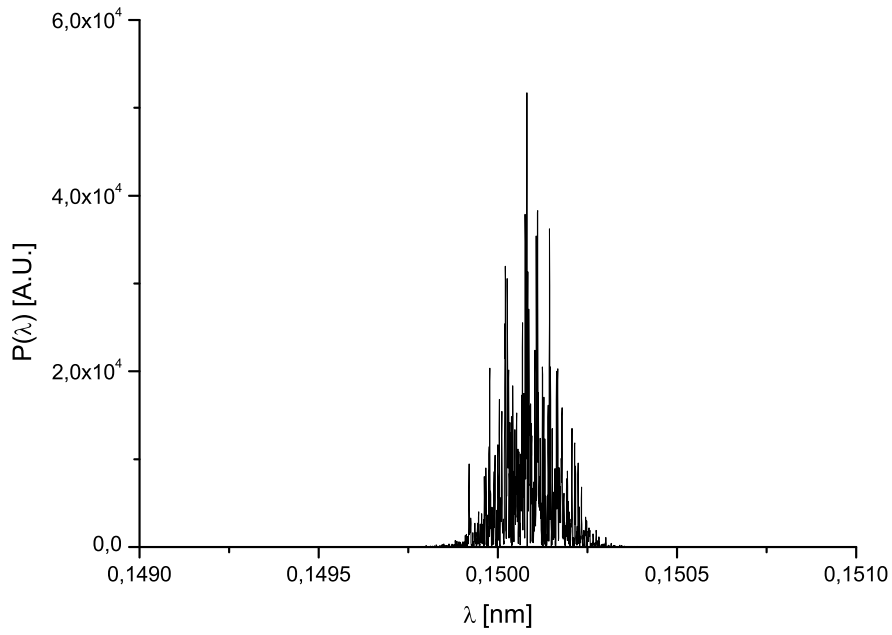


Fig. 49. Long pulse mode operation. Combination of self-seeding and fresh bunch techniques. Spectrum at the end of the second stage, 7 cells long (42 m).

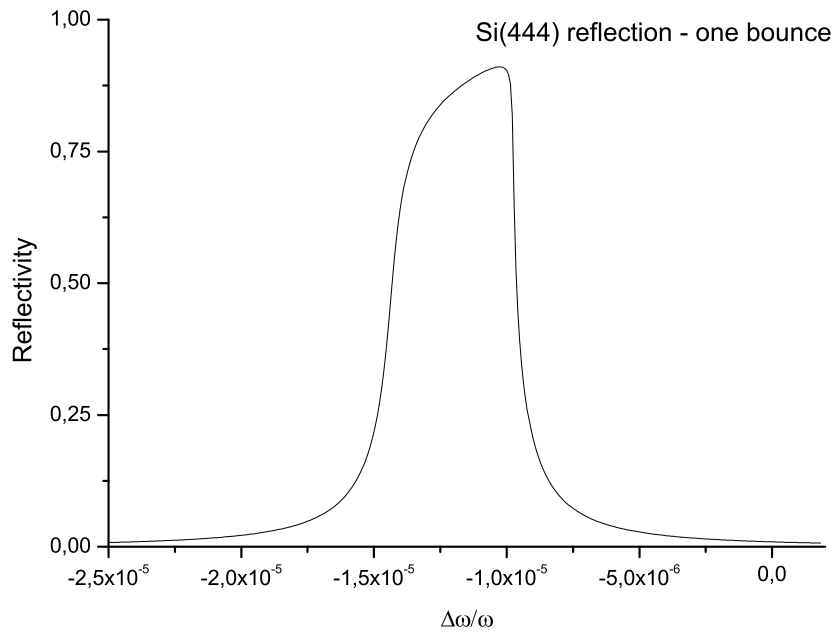


Fig. 50. Reflectivity curve for a thick absorbing crystal in Bragg geometry. Si(444) reflection of 0.15 nm X-rays. One bounce.

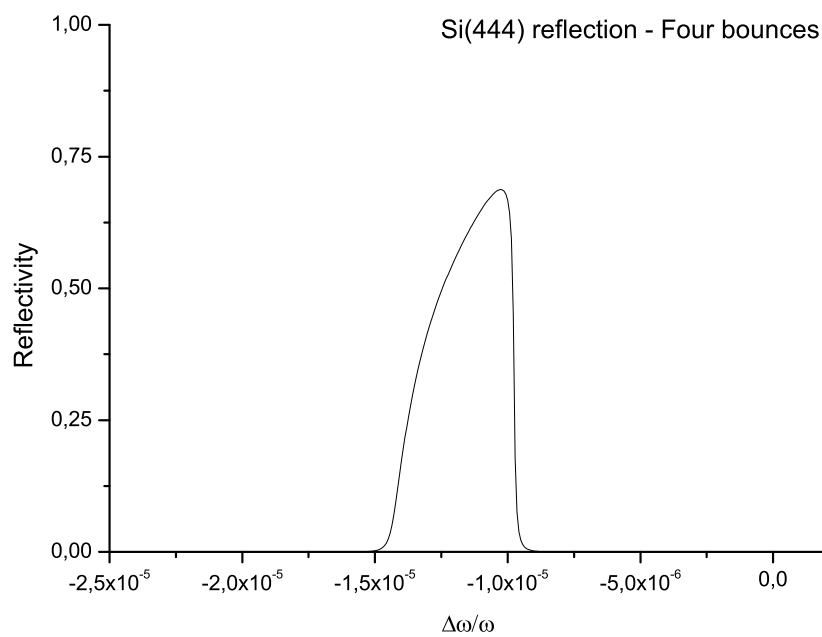


Fig. 51. Reflectivity curve for a thick absorbing crystal in Bragg geometry. Si(444) reflection of 0.15 nm X-rays. Four bounces.

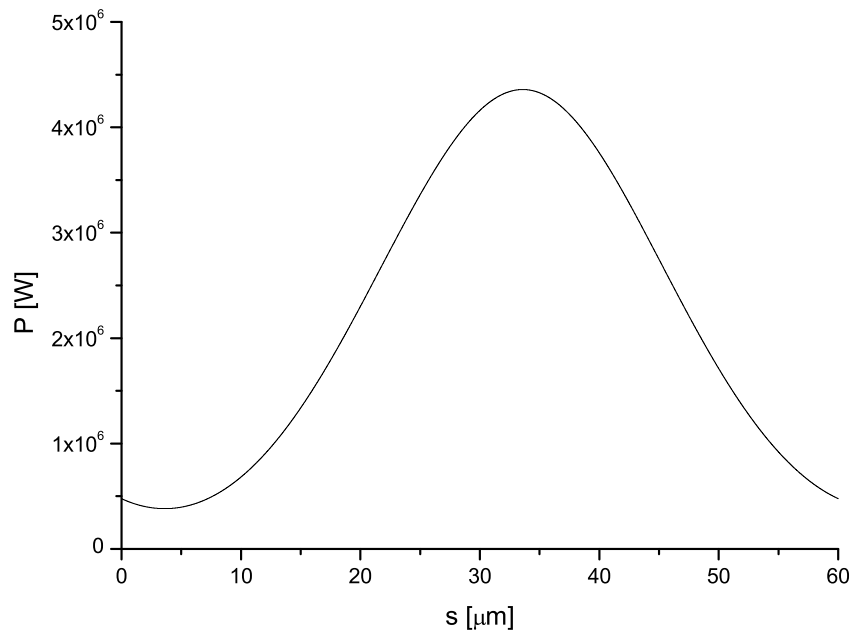


Fig. 52. Long pulse mode of operation, combination of self-seeding and fresh bunch techniques. Power after the four-bounce monochromator, Si(444) reflection. Radiation is used as input for the third undulator part.

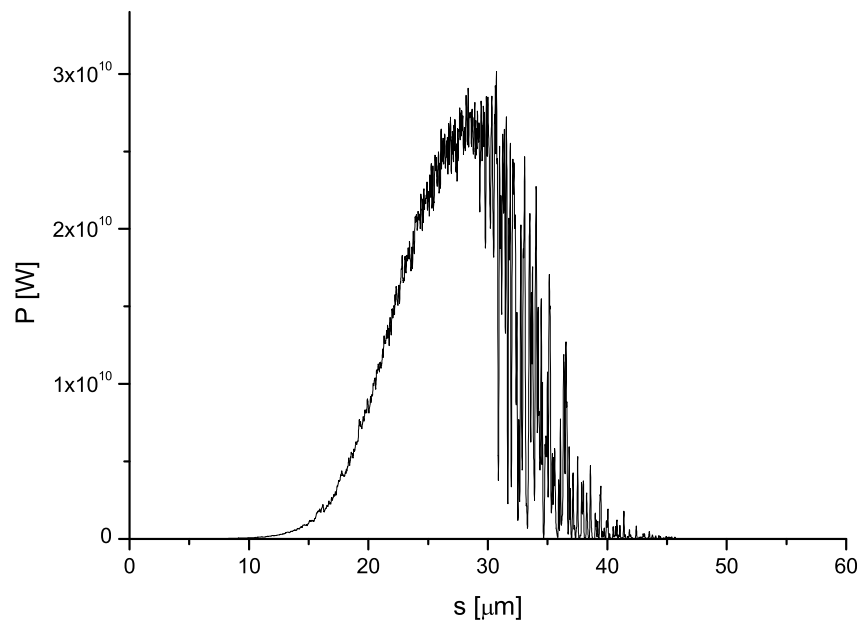


Fig. 53. Long pulse mode operation, combination of self-seeding and fresh bunch techniques with a Si(444) reflection, four-bounce monochromator. Power at the end of the third stage, 7 cells long (42 m).

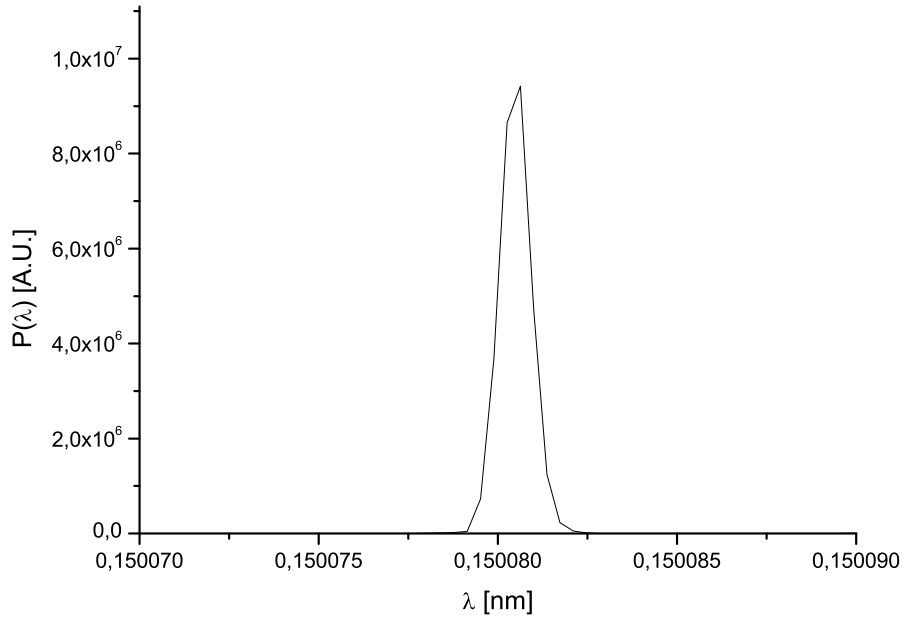


Fig. 54. Long pulse mode operation, combination of self-seeding and fresh bunch techniques with a Si(444) reflection, four-bounce monochromator. Spectrum at the end of the third stage, 7 cells long (42 m).

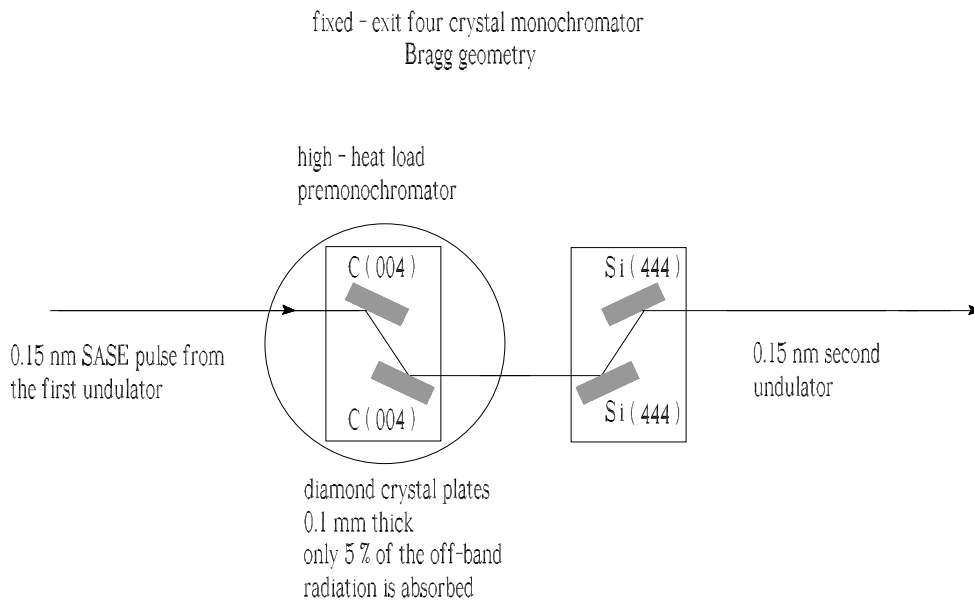


Fig. 55. Four bounce scheme for the X-ray monochromator. It allows one to use the first two Bragg reflectors as a high-heat load premonochromator. In the premonochromator part one can use diamond crystal plates 100 $\mu$ m-thick and the Bragg reflection C(004).



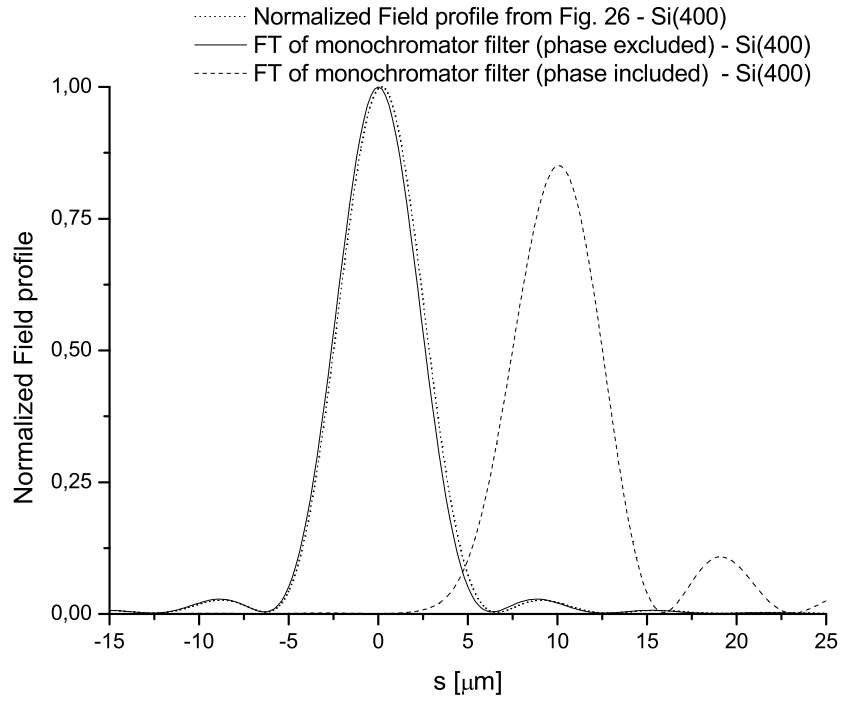


Fig. 56. Normalized field profile after the four-bounce Si(400) reflections for the short bunch case, single shot. We compare the results from Fig. 26 with the Fourier transform of the monochromator filter with and without phase.